OSU

The Ohio State University

ANALYSIS OF AIRBORNE ANTENNA SYSTEMS USING GEOMETRICAL THEORY OF DIFFRACTION AND MOMENT METHOD COMPUTER CODES

By

Richard G. Hartenstein, Jr.

The Ohio State University

ElectroScience Laboratory

Department of Electrical Engineering
Columbus, Ohio 43212

Technical Report No. 716199-6
Grant No. NSG 1498
August 1985

National Aeronautics and Space Administration
Langley Research Center
Hampton, Virginia 23665

NOTICES

When Government drawings, specifications, or other data are used for any purpose other than in connection with a definitely related Government procurement operation, the United States Government thereby incurs no responsibility nor any obligation whatsoever, and the fact that the Government may have formulated, furnished, or in any way supplied the said drawings, specifications, or other data, is not to be regarded by implication or otherwise as in any manner licensing the holder or any other person or corporation, or conveying any rights or permission to manufacture, use, or sell any patented invention that may in any way be related thereto.

50272-101

REPORT DOCUMENTATION PAGE	1. REPORT NO.	2.	3. Recipient's Accession No.

4. Title and Subtitle

ANALYSIS OF AIRBORNE ANTENNA SYSTEMS USING GEOMETRICAL THEORY OF DIFFRACTION AND MOMENT METHOD COMPUTER CODES

5. Report Date

August 1985

6.

7. Author(s)

R.G. Hartenstein, Jr.

8. Performing Organization Rept. No.

716199-6

9. Performing Organization Name and Address

The Ohio State University
ElectroScience Laboratory
1320 Kinnear Road
Columbus, Ohio 43212

10. Project/Task/Work Unit No.

11. Contract(C) or Grant(G) No.

(C)
(G) (G) NSG 1498

12. Sponsoring Organization Name and Address

National Aeronautics and Space Administration
Langley Research Center
Hampton, Virginia 23665

13. Type of Report & Period Covered

Technical

14.

15. Supplementary Notes

16. Abstract (Limit: 200 words)

Computer codes have been developed to analyze antennas on aircrafts and in the presence of scatterers. The purpose of this study is to use these codes to develop accurate computer models of various aircraft and antenna systems. The antenna systems analyzed are a P-3B L-Band antenna, an A-7E UHF relay pod antenna, and traffic advisory antenna system installed on a Bell Long Ranger helicopter. Computer results are compared to measured ones with good agreement. These codes can be used in the design stage of an antenna system to determine the optimum antenna location and save valuable time and costly flight-hours.

17. Document Analysis a. Descriptors

b. Identifiers/Open-Ended Terms

c. COSATI Field/Group

18. Availability Statement	19. Security Class (This Report)	21. No. of Pages
	Unclassified	69
	20. Security Class (This Page) Unclassified	22. Price

(See ANSI-Z39.18) See Instructions on Reverse OPTIONAL FORM 272 (4-77) (Formerly NTIS-35) Department of Commerce

TABLE OF CONTENTS

LIST OF TABLES

LIST OF FIGURES

CHAPTER I

INTRODUCTION

The success of an airborne avionics system is critically dependent on its antenna system. The antenna system provides the vital link from the aircraft to the ground station or another aircraft. The antenna performance is affected by the aircraft structure, and its radiation pattern will depend on the antenna location. Many times an antenna will be arbitrarily placed on an aircraft only to find that after many costly hours of flight time that the antenna coverage is inadequate.

Computer codes have been developed to analyze antennas on an aircraft or in the presence of scatterers. Using these codes, the performance of an airborne antenna can be modelled during the development stage of the system, thus saving costly flight time. The codes can also be used to help determine the causes of a problem in the radiation coverage of an existing system.

The purpose of this study is to use these codes to develop accurate computer models of various aircraft. The codes are used to analyze airborne antenna radiation patterns which are then compared to measured results. Three codes are used throughout this study; the Airborne Antenna Code, the Basic Scattering Code and the Electromagnetic Surface Patch Code. These codes are described in Chapter II.

An L-band antenna installed on a P-3B aircraft is analyzed in Chapter III. A UHF relay pod antenna mounted on an A-7E aircraft is analyzed in Chapter IV. A traffic advisory antenna system installed on Bell Long Ranger helicopter is analyzed in Chapter V. Finally, Chapter VI contains a summary and conclusions.

CHAPTER II

SUMMARY OF COMPUTER CODES

A. INTRODUCTION

This chapter briefly describes the three computer codes used to generate the theoretical results of this study. The basic capabilities of each code are summarized in Table I. The Airborne Antenna Code and

TABLE I
CODES AND BASIC CAPABILITIES

CODE	CAPABILITIES
AIRBORNE ANTENNA CODE	Near- or far-field patterns of antennas mounted on a aircraft or similar structure. Used for slots, stubs or arrays mounted on an aircraft fuselage or convex surface.
BASIC SCATTERING CODE	Far-field patterns of antennas in the presence of conducting scattering structures. Used, for example, for antennas on a ship, truck, aircraft, etc. The antennas can not be mounted on a curved surface which complements the Airborne Antenna Code.
ELECTROMAGNETIC SURFACE PATCH CODE	Far-field or scattering patterns of antennas in the presence of wires and/or plates. Can be used to determine mutual coupling effects. It is limited to structures that are small in terms of the wavelength. It complements the two previous codes in that they require electrically large structures.

Basic Scattering Code were developed using the Uniform Geometrical Theory of Diffaction. The Electromagnetic Surface Patch Code implements a moment method solution. Each code is described in some detail in the following sections.

B. AIRBORNE ANTENNA CODE

The Airborne Antenna Code is a Fortran IV computer code developed to determine the radiation patterns of antennas mounted on a perfectly conducting composite ellipsoid in the presence of a set of finite, perfectly conducting flat plates. The analysis of the antenna radiation patterns is based on the Uniform Geometrical Theory of Diffraction (UTD) [1,2,3]. This code is applied to aircraft by modelling the fuselage as an ellipsoid and adding flat plates to simulate the wings, vertical stabilizer, and any other scattering structure that may be present. The flat plates can be attached to the fuselage and/or to each other.

The Airborne Antenna Code can calculate arbitrary conical azimuthal and great-circle elevation patterns. The code can analyze radial monopoles, up to a quarter-wavelength long, and arbitrarily oriented slot antennas. Mutual coupling effects, for example, between two monopoles can be accomplished with the help of a moment method solution. Image theory can be applied to model the monopoles as dipoles and to calculate the relative current distribution. The relative currents are then input into the Airborne Antenna Code as two sources. The radiation pattern from the second source is superimposed on the pattern of the primary source for the final pattern.

The Airborne Antenna Code calculates and superimposes a number of different fields for each given geometry. The total field is made up of first-order and second-order fields. The first-order fields are the source, reflected, and diffracted terms; whereas, the second-order fields are the reflected/reflected, diffracted/reflected, reflected/diffracted and diffracted/diffracted ones. These various terms are illustrated in Figure 2.1. Any higher-order terms caused by additional interactions are assumed to be insignificant compared to the dominants ones and are not included in this code. The code calculates only the first-order terms unless the user specifies that the second-order terms are to be included.

Because UTD is a high frequency solution, only the most basic structural features of the aircraft need to be modeled. Ray optical techniques are used to determine the field incident on and reflected by the various structures. The diffracted fields are found using UTD and are summed with the geometrical optics field at an observation point. To determine the field at a given observation point, a ray path must be determined. This path can be the direct source radiation, reflection from a plate, diffraction from an edge, or via a second-order mechanism trajectory. Each path is determined using the laws of reflection and diffraction. It is then determined if the path is shadowed by any structures. If the path is shadowed, the field is not computed, and the code proceeds to the next scatterer or observation point. If the path is not shadowed, the field is computed and added to the total field.

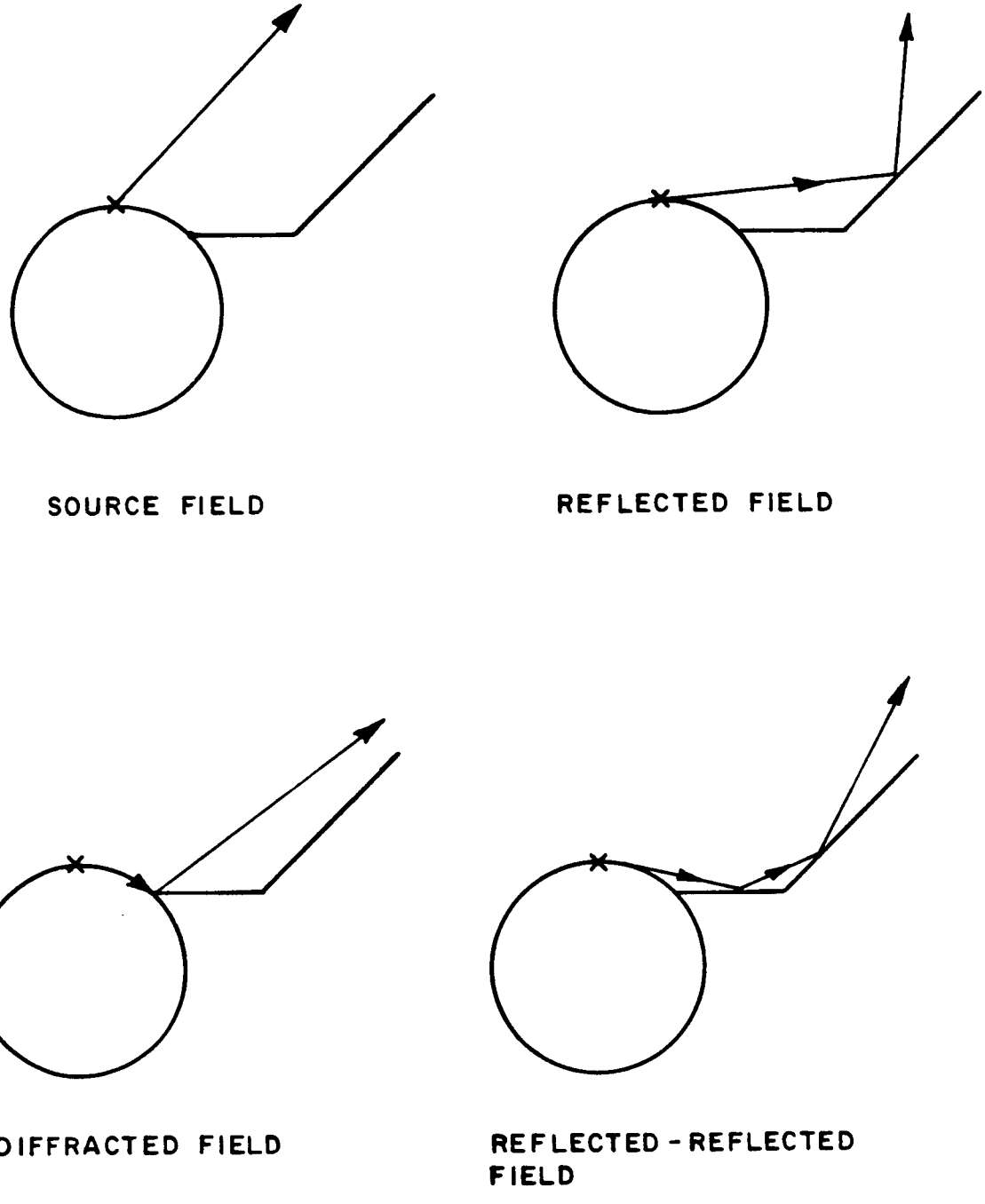

Figure 2.1. Various GTD terms calculated in the Airborne Antenna Code.

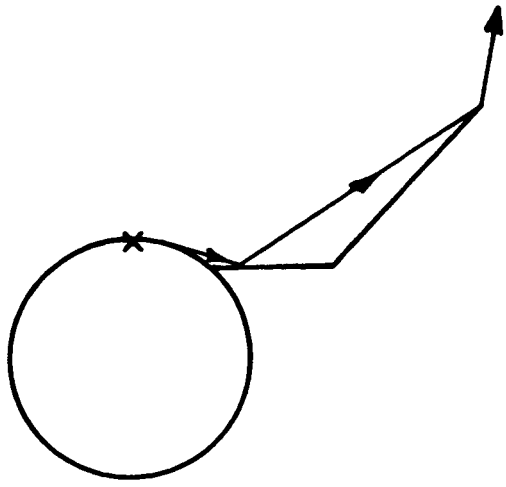

REFLECTED - DIFFRACTED FIELD

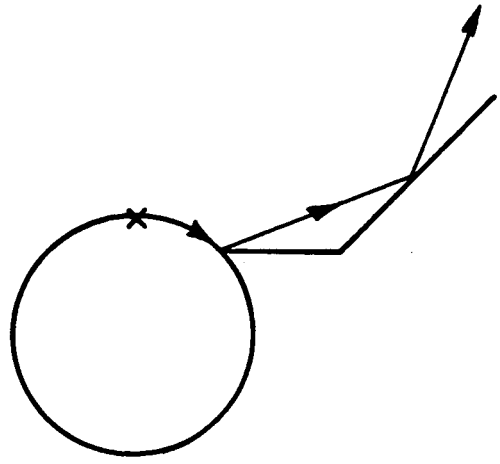

DIFFRACTED - REFLECTED FIELD

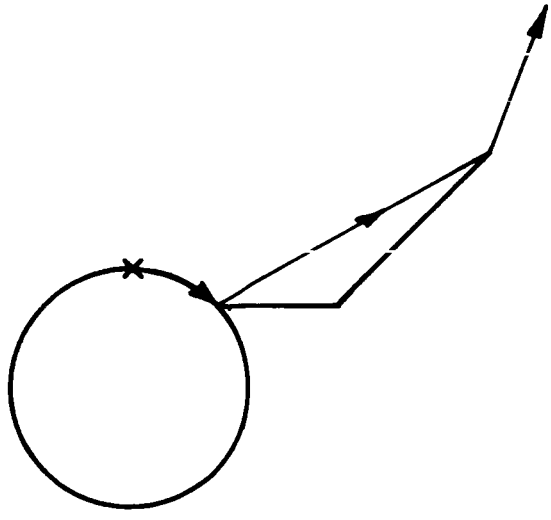

DIFFRACTED - DIFFRACTED FIELD

Figure 2.1. (continued).

This approach of shadowing rays might lead to various discontinuities in the resulting pattern, but the UTD solution is designed to avoid these discontinuities. The UTD diffraction coefficients smooth out the discontinuities to produce a continuous field. If discontinuities still exist, it usually indicates that higher-order terms need to be included.

Because of the nature of the UTD analysis, there are limitations associated with the Airborne Antenna Code. Each plate should have edges at least a wavelength long. The radii of the ellipsoid should be at least a wavelength long, and each antenna should be at least a wavelength from any plate edge. In many cases, this limit can be reduced to a quarter wavelength for engineering purposes.

The Airborne Antenna Code is user-oriented in that the user can run the code without knowing all the details of its operation. The user need only be familiar with the input, output, capabilities and limitations of the code so that he can properly interpret its results. More information on the use of the code can be found in reference [4].

C. BASIC SCATTERING CODE

The Basic Scattering Code (BSC) is a Fortran IV computer code developed for the electromagnetic analysis of the radiation from antennas in the presence of complex structures. The code has the capability to predict far- and near-field radiation patterns as well as

coupling between antennas in the presence of scattering structures. In addition, it can be used to determine potential radiation hazards. The scattering structures are simulated by piecing together perfectly conducting flat plates, finite elliptic cylinders and finite thin dielectric slabs.

The BSC can model a wide variety of antennas. A source can be specified as an electric or magnetic type. For a given source type, three different current distributions can be simulated. They are the uniform, sinusoidal, and standard TE_{01} mode (cavity back slot) current distributions. An aperture width can be specified or set equal to zero in the case of a dipole antenna. If all scattering centers are in the far-field of the antenna, the antenna can be represented by its pattern factor to save computer time. Similarly, an array can be represented by its array factor. The BSC can account for mutual coupling effects in the same manner that was described for the Airborne Antenna Code.

Like the Airborne Antenna Code, the analysis used is based on the Uniform Geometrical Theory of Diffraction. Therefore, the solution is constructed in a similar manner. A ray path is determined by the laws of reflection and diffraction, and if no structure blocks the ray path, then the field is computed at the observation point. The total field contains source, reflected, diffracted, reflected/reflected, reflected/diffracted, and diffracted/reflected terms. The second-order terms include interactions between two plates, between two cylinders, and between a plate and cylinder. The various terms are illustrated in Figure 2.2.

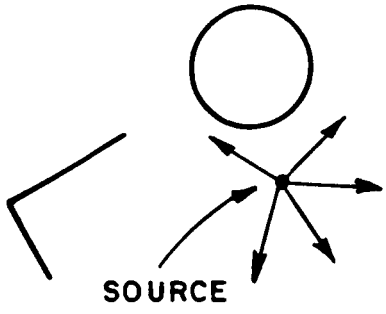

SOURCE FIELD

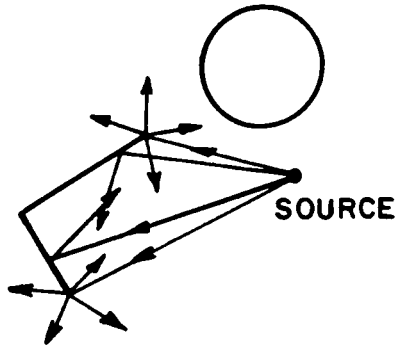

PLATE REFLECTED AND
PLATE DIFFRACTED

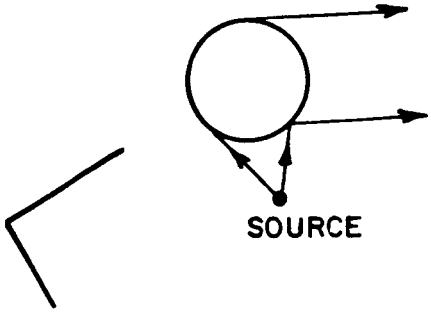

CYLINDER REFLECTED AND
CYLINDER DIFFRACTED

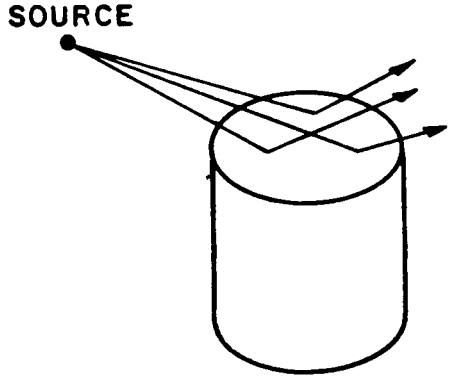

CYLINDER END
CAP REFLECTED

Figure 2.2. Various GTD terms calculated in the Basic Scattering Code.

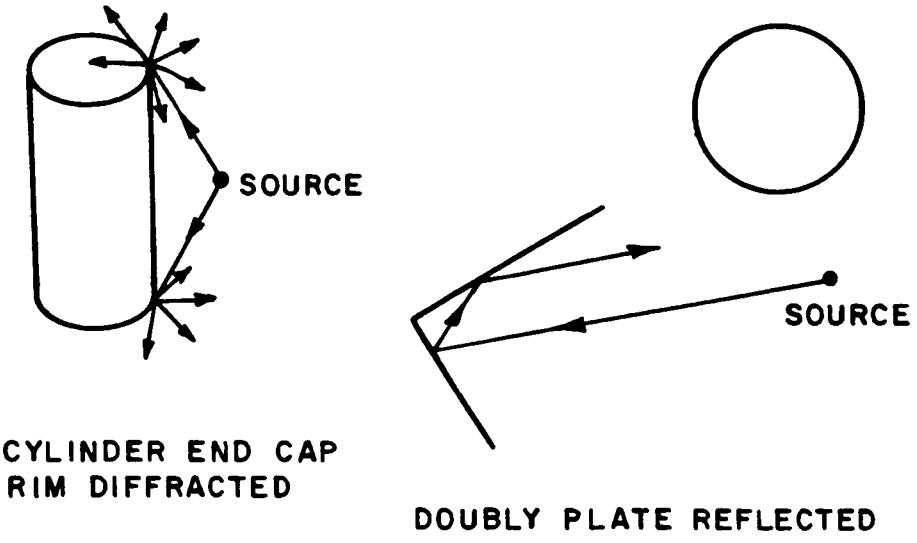

CYLINDER END CAP
RIM DIFFRACTED

DOUBLY PLATE REFLECTED

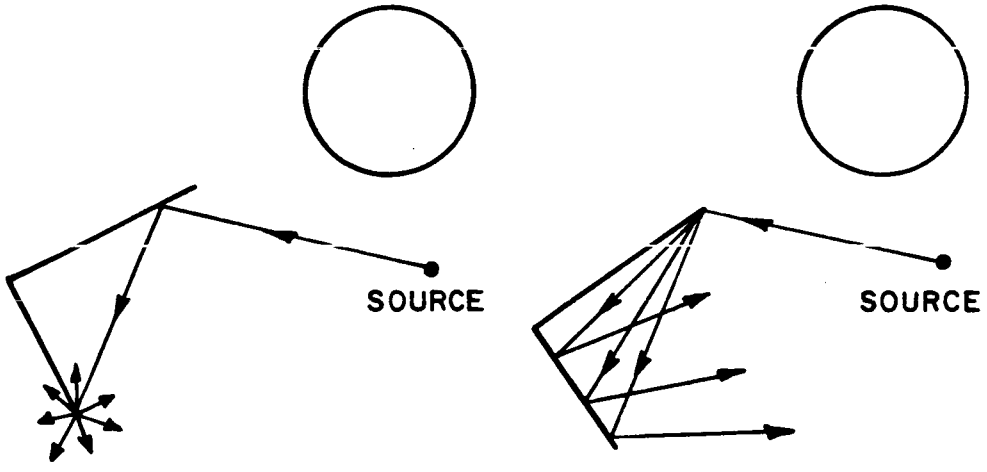

PLATE REFLECTED /
PLATE DIFFRACTED

PLATE DIFFRACTED /
PLATE REFLECTED

Figure 2.2. (continued).

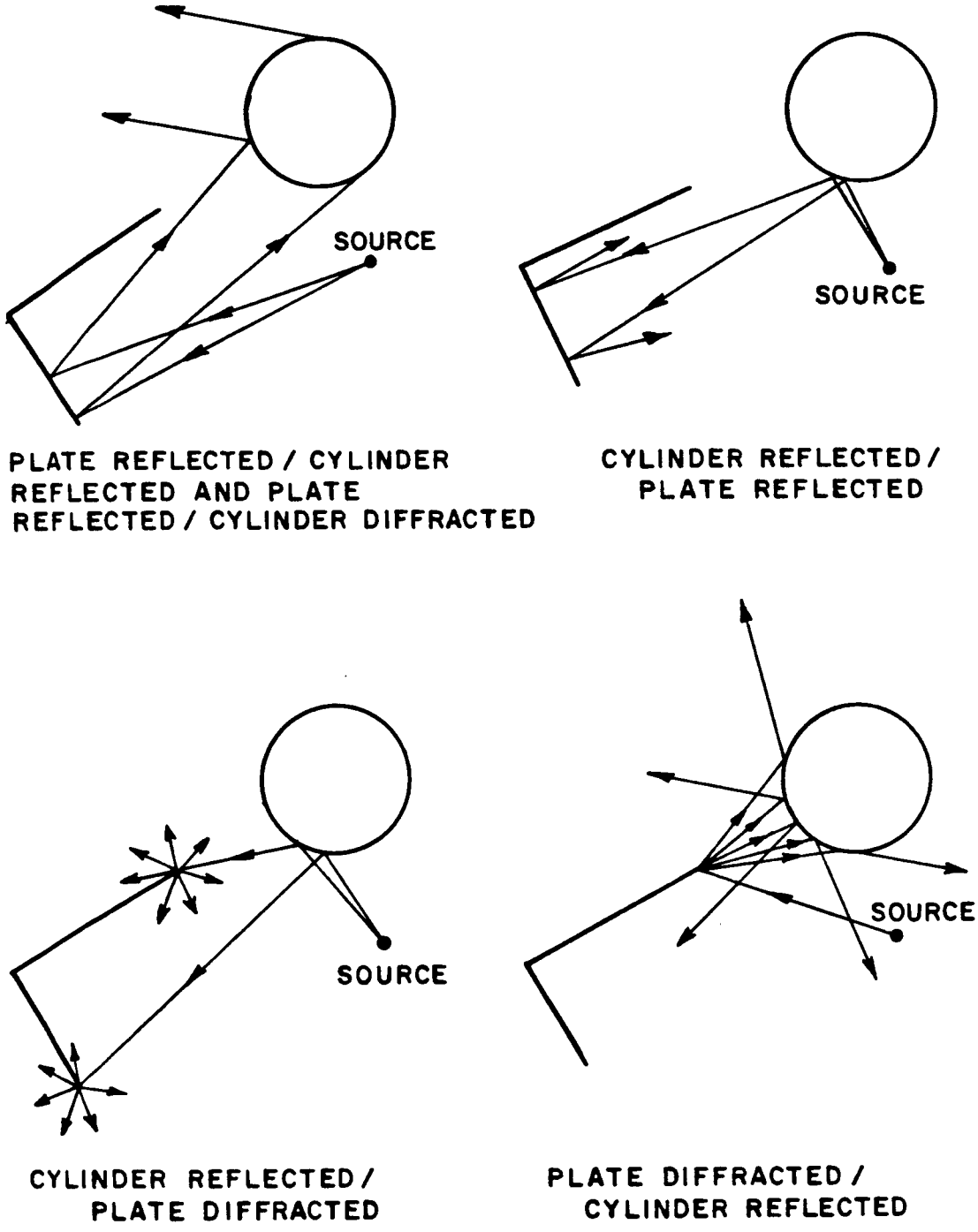

Figure 2.2. (continued).

Because this code is also derived from the UTD, its limitation are similar to those of the Airborne Antenna Code. Each plate should have edges at least a wavelength long. The length, and major and minor radii of each cylinder should be at least a wavelength. Each antenna element should be a wavelength from all edges. If a dielectric slab is used, the source should be a wavelength from the slab and the incident field should not strike the slab too close to grazing.

The BSC is designed to be user-oriented. A user can run the code with a minimum amount of knowledge of how the code operates. However, the user should have a basic understanding of the input, output, capabilities, and limitations so he can properly define the input and interpret the results. Details on the use and operations of the BSC can be found in the User's [5] and Code [6] Manuals.

D. ELECTROMAGNETIC SURFACE PATCH CODE

The Electromagnetic Surface Patch (ESP) Code is a Fortran IV computer code which applies a moment method solution to thin wires and rectangular plates. The purpose of the code is to model antennas with thin wires and any supporting structure or scatterer with flat plates and/or thin wires. Wires can be attached to plates, and plates can be attached to plates. The wires can be fed by arbitrary complex voltages or loaded by complex impedances. The code computes the currents induced on each wire and plate, the antennas input impedance and admittance, and its efficiency. The ESP code can compute the far-field antenna

radiation patterns, both theta and phi polarizations. For a scattering problem, the code can compute either the backscattered or bistatic scattered patterns for theta, phi and cross polarizations. The code produces either great-circle elevation or conical azimuthal patterns. Finally, the code can plot the wire/plate geometry as well as the calculated patterns.

To find the currents, each wire is divided into segments. Two adjacent wire segments make up a wire dipole mode. Similarly, each plate is divided into smaller rectangular segments. The rectangular segments are paired with adjacent rectangular segments to form surface patch dipole modes. These two current modes are illustrated in Figure 2.3. The limitations associated with this code are mainly placed on the size of these segments. The length of each wire segment and the length and width of each plate segment should be limited to a quarter wavelength. Also, any attachment point between a wire and a plate should be at least a tenth of a wavelength from the edge of the plate.

The ESP code is also a user-oriented code. The user need only define the wire and plate geometries, type of computation desired, and a few various other parameters to execute the program. Information on the use of the ESP code can be found in the user's manual [7].

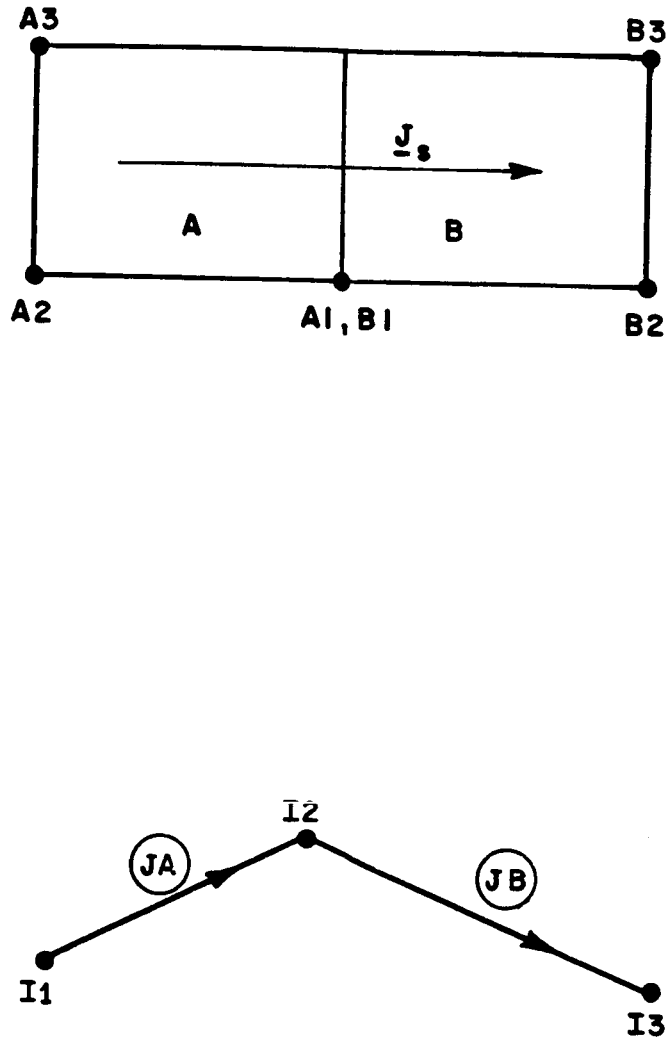

Figure 2.3. Current modes calcualted in the Electromagnetic Surface Patch Code.

CHAPTER III

P-3B L-BAND ANTENNA ANALYSIS

In this chapter the Airborne Antenna and the ESP Codes are applied to simulate a P-3B antenna problem. The P-3B, shown in Figure 3.1, is a four-turboprop anti-submarine aircraft equipped with numerous avionic systems. Among these is an L-band antenna located on the belly of the aircraft as illustrated in Figure 3.2. An omnidirectional radiation pattern in the azimuth plane is desired for this application. However, as Figure 3.3 shows, the radiation pattern is fairly omnidirectional except for the rear quadrant where the gain is reduced by 4-6 dB. The measured data shown in Figure 3.3 was taken in flight at the Naval Air Test Center (Patuxent River, Maryland).

Using the Airborne Antenna Code, the L-band antenna was modelled as a quarter-wave monopole attached to an ellipsoid with 17 plates added to simulate the wings, horizontal stabilizers, and engine housings. Figure 3.4 shows a diagram of the computer model. The results of this simulation are shown in Figure 3.5 with the measured results. The calculated radiation pattern is fairly omnidirectional with some constructive interference from the wings. Compared to the measured pattern, the calculated pattern agrees very well in the front quadrant;

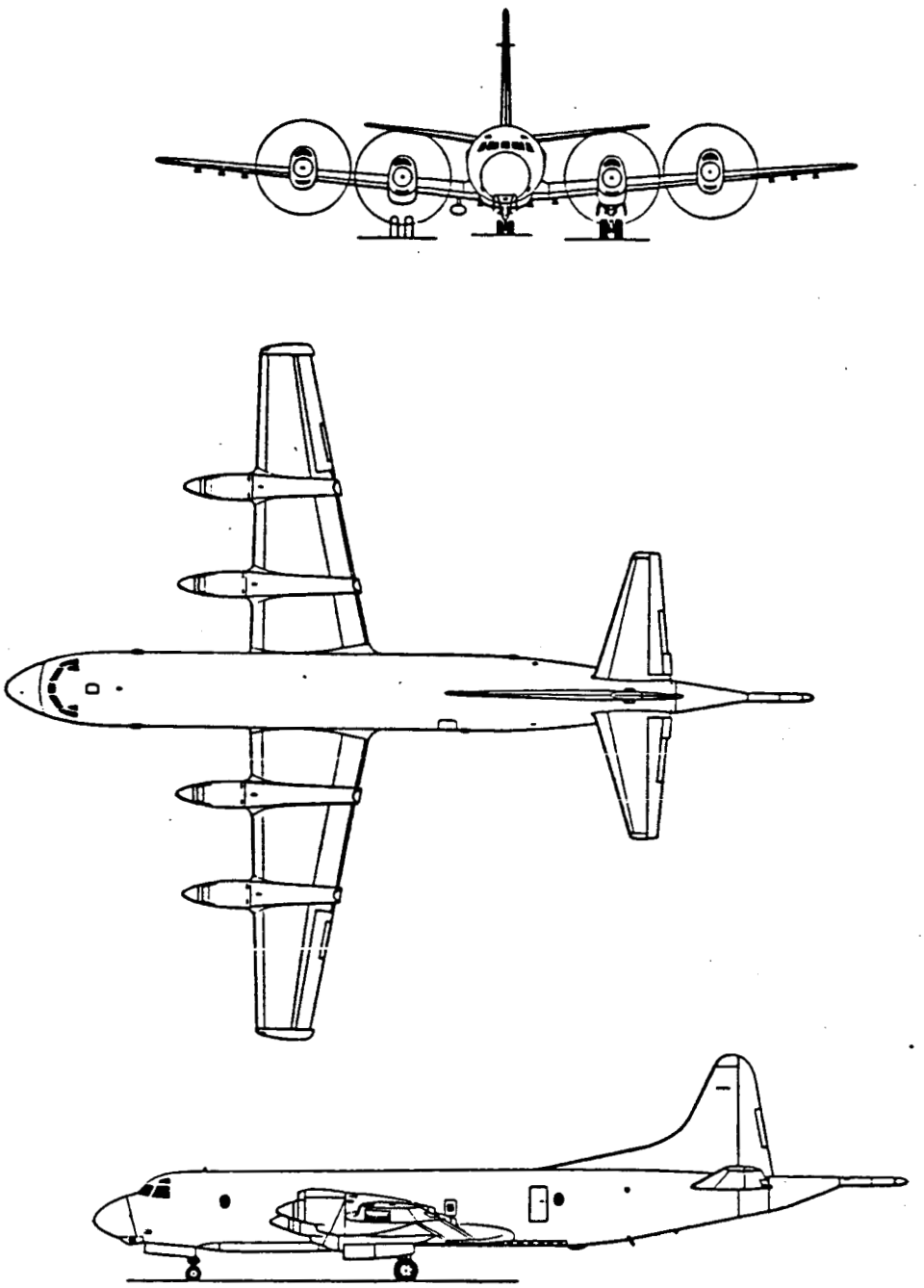

Figure 3.1. P-3B line drawing.

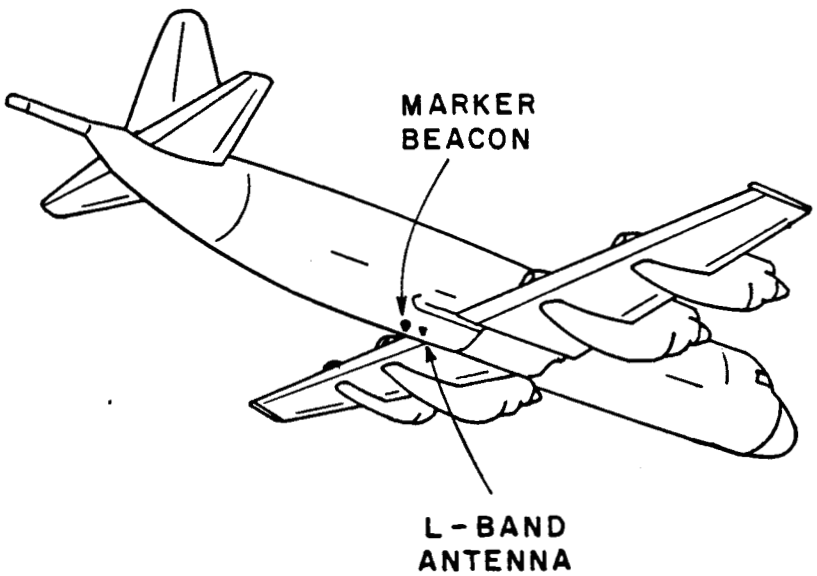

Figure 3.2. P-3B L-band antenna location.

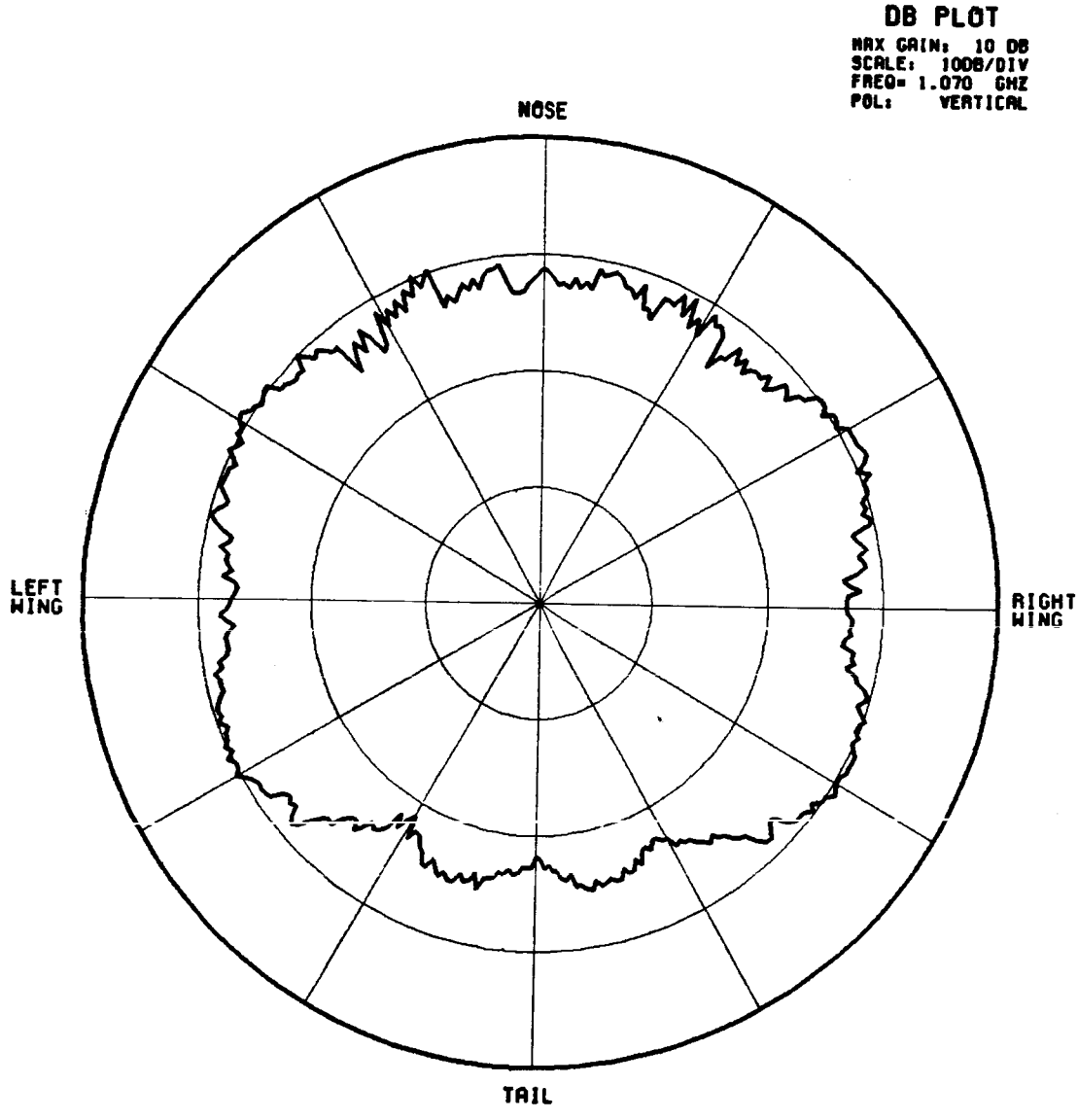

Figure 3.3. Measured P-3B azimuth L-band antenna radiation pattern.

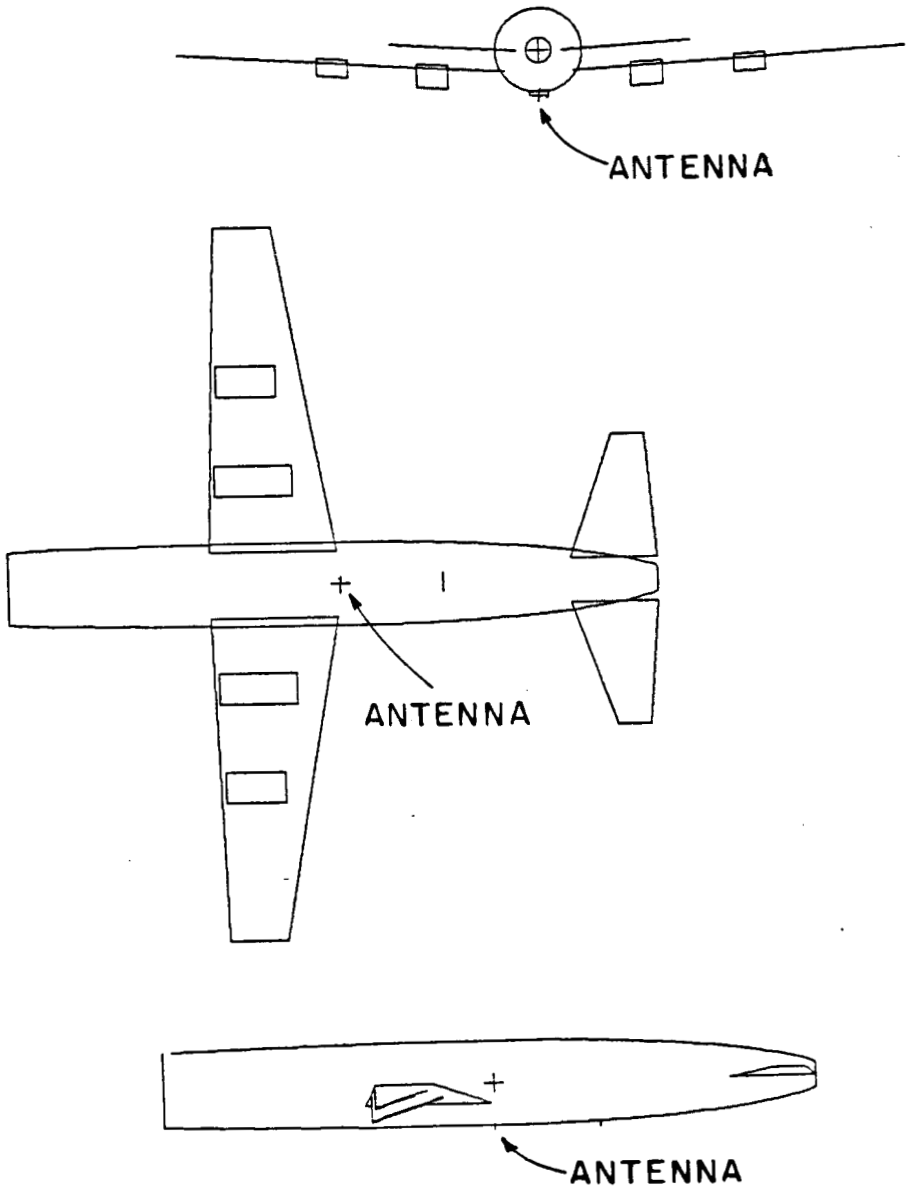

Figure 3.4. P-3B computer model.

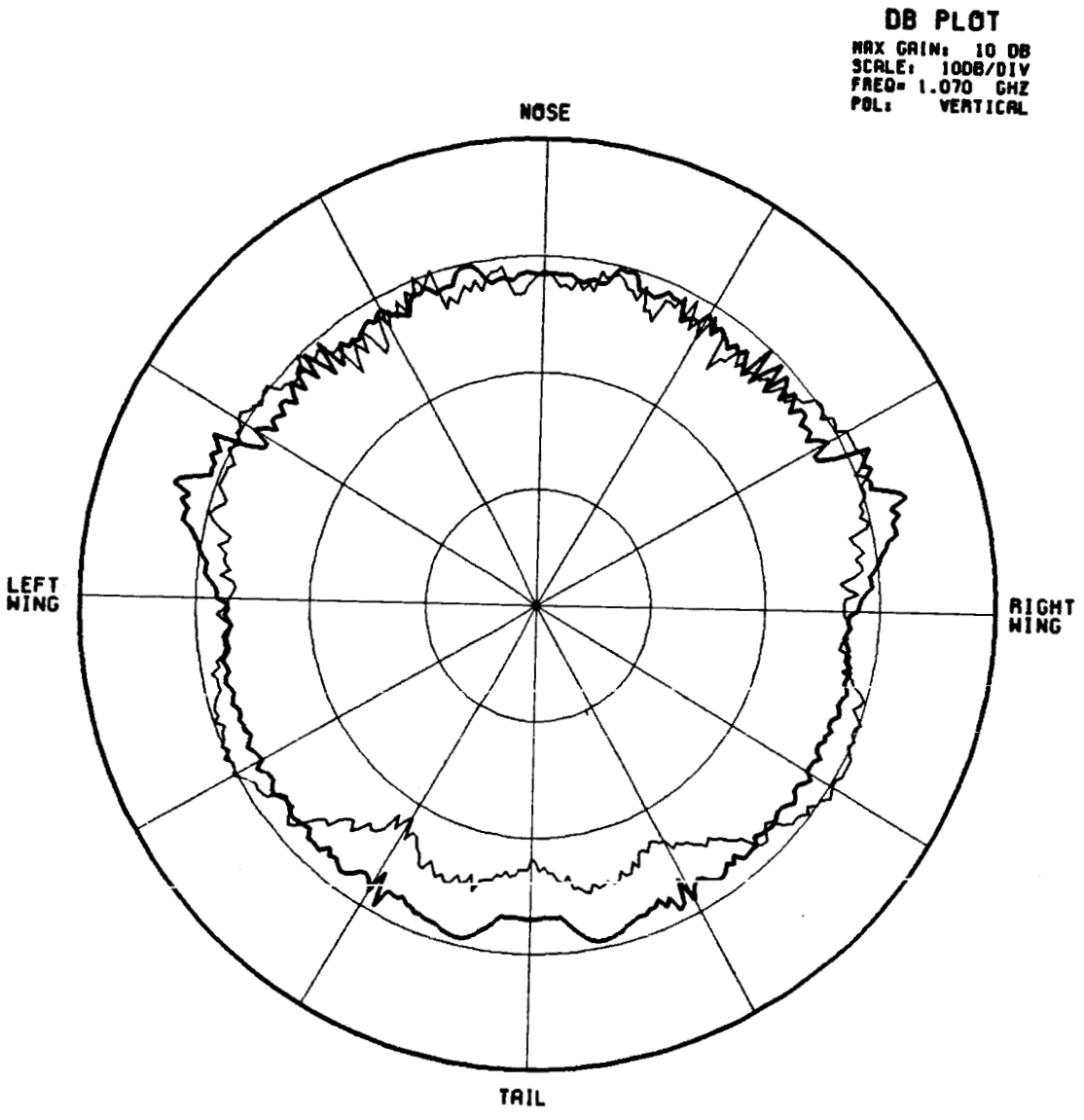

Figure 3.5. P-3B azimuth L-band antenna radiation pattern.
Calculated (using single source)
Measured

however in the side quadrants, the patterns differ by as much as 2-3 dB and in the rear quadrant by as much as 6 dB.

Closer examination of the P-3B belly shows a marker beacon located only 11 inches (less than one wavelength) behind the antenna. Here, the ESP code was used to model the antenna and beacon as a mutual coupling problem, as if currents were being induced on the beacon and reradiating. Using image theory in the ESP code, the monopole was modelled as a dipole in free-space. Since the Airborne Antenna Code analyzes only radial monopoles or slot antennas, the beacon was modelled as a shorted dipole in the ESP code. The source dipole was placed in front of the shorted dipole as shown in Figure 3.6. A listing of the ESP code input file for this geometry is shown in Figure 3.7. Figure 3.8 shows the ESP code output file. The ESP code calculated a relative complex current of -0.179-j0.155 on the shorted dipole compared to 0.970-j0.242 on the source dipole. These value are taken from mode 5 and mode 2 as indicated in the boxes on page 26. Mode 5 is the center mode of the shorted dipole and mode 2 is the center mode of the source dipole.

The current of mode 5 relative to mode 2 was then input into the Airborne Antenna Code as a second source, and the results were superimposed on the single source pattern. These results are compared to the measured results in Figure 3.9. This comparison shows very good agreement throughout the pattern except in the rear quadrant where the difference was reduced to 1-3 dB. It also shows that the computer model did well to simulate the coupling effect of the beacon, but not as well

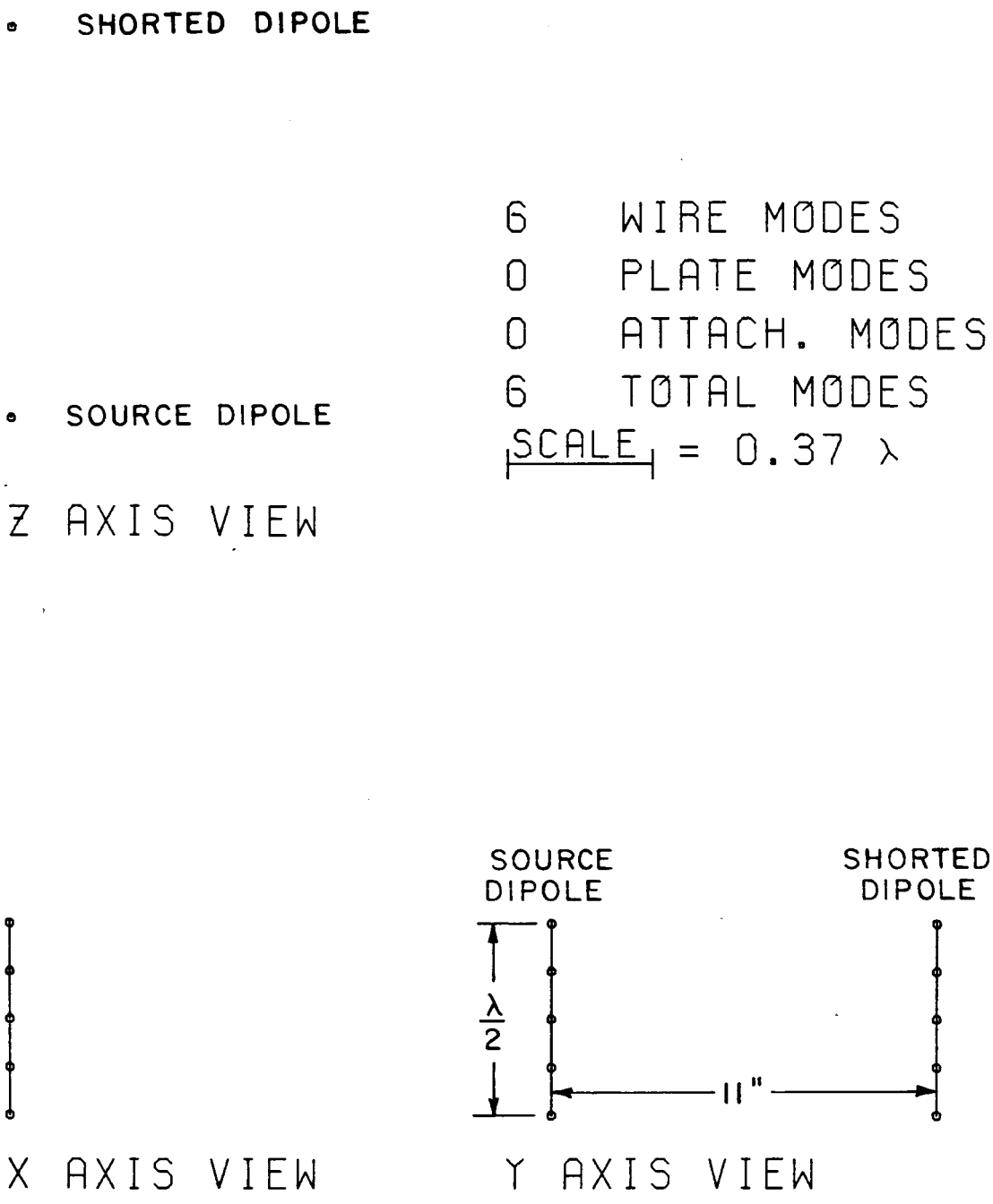

Figure 3.6. Monopole/beacon simulation geometry.

```
1  2  1  1  1  0  4  10  18  1  1
0  0  1  0.0
1  0  1  90.0
0  0  1  0.0  90.0  0.0
0  0  1  0.0
1070.0  -1  0.00025
0  0
0  0
8        10       0        1
0.0      0.0      -.0688   !DIPOLE
0.0      0.0      -.0344
0.0      0.0      0.0
0.0      0.0      0.0344
0.0      0.0      0.0688
-.2794   0.0      -.0688   !BEACON
-.2794   0.0      -.0344
-.2794   0.0      0.0
-.2794   0.0      0.0344
-.2794   0.0      0.0688
1        2
2        3
3        4
4        5
6        7
7        8
8        9
9        10
3  0  (1.0,0.0)  (0.0,0.0)
```

Figure 3.7. ESP code input file for monopole/beacon simulation.

```
        INPUT DATA

FREQ.(MHZ) =  1070.000
WAVE(M) =      0.280

WIRE RADIUS(M) =  0.0002500
INTP=  10
INTD=  18
INT =    4


WIRE CONDUCTIVITY = -1.00 MEGAMHOS/M


  10 POINTS ON THE WIRE
 I          X (I)          Y (I)          Z (I)

 1    0.0000E+00     0.0000E+00    -0.6880E-01
 2    0.0000E+00     0.0000E+00    -0.3440E-01
 3    0.0000E+00     0.0000E+00     0.0000E+00
 4    0.0000E+00     0.0000E+00     0.3440E-01
 5    0.0000E+00     0.0000E+00     0.6880E-01
 6   -0.2794E+00     0.0000E+00    -0.6880E-01
 7   -0.2794E+00     0.0000E+00    -0.3440E-01
 8   -0.2794E+00     0.0000E+00     0.0000E+00
 9   -0.2794E+00     0.0000E+00     0.3440E-01
10   -0.2794E+00     0.0000E+00     0.6880E-01


 MODES ON THE WIRE STRUCTURE

 MAXIMUM NUMBER OF MODES AT ONE POINT =  2
 MINIMUM NUMBER OF MODES AT ONE POINT =  1
 NUMBER OF WIRE MODES =  6


 I  I1(I)  I2(I)  I3(I)  JA(I)  JB(I)

1      1      2      3      1      2
2      2      3      4      2      3
3      3      4      5      3      4
4      6      7      8      5      6
5      7      8      9      6      7
6      8      9     10      7      8
```

Figure 3.8. ESP code output file for monopole/beacon simulation.

```
  8 SEGMENTS ON THE WIRE
 J     IA(J)    IB(J)     D(J) (M)

 1       1        2      0.34400E-01
 2       2        3      0.34400E-01
 3       3        4      0.34400E-01
 4       4        5      0.34400E-01
 5       6        7      0.34400E-01
 6       7        8      0.34400E-01
 7       8        9      0.34400E-01
 8       9       10      0.34400E-01


 LISTING OF LOADS AND GENERATORS

  0.1000E+01    0.0000E+00 VOLTS BY PT. A OF SEGMENT    3


 NWR = NUMBER OF WIRE MODES =     6
 NPLTM = NUMBER OF PLATE MODES =     0
 NAT = NUMBER OF ATTACHMENT MODES =     0


  ANTENNA MODAL CURRENTS
MODE    REL MAG       ABS MAG       PHASE          *** COMPLEX ***

  1      0.755       0.0092660       -20.       0.008728      -0.003112
  2      1.000       0.0122726       -14.       0.011894      -0.003026
  3      0.755       0.0092660       -20.       0.008728      -0.003112
  4      0.174       0.0021398      -139.      -0.001616      -0.001403
  5      0.237       0.0029130      -139.      -0.002203      -0.001906
  6      0.174       0.0021398      -139.      -0.001616      -0.001403

 INPUT ADMITTANCE(MHOS) =    0.011894 J  -0.003026
 INPUT IMPEDANCE(OHMS) =      78.966 J     20.093
 EFFICIENCY(PERCENT) = 100.000


 CPU RUN TIME FOR RUN   1 GEOMETRY   1 =         7.69 SECONDS

 TOTAL CPU RUN TIME =          7.86 SECONDS
```

Figure 3.8. (continued).

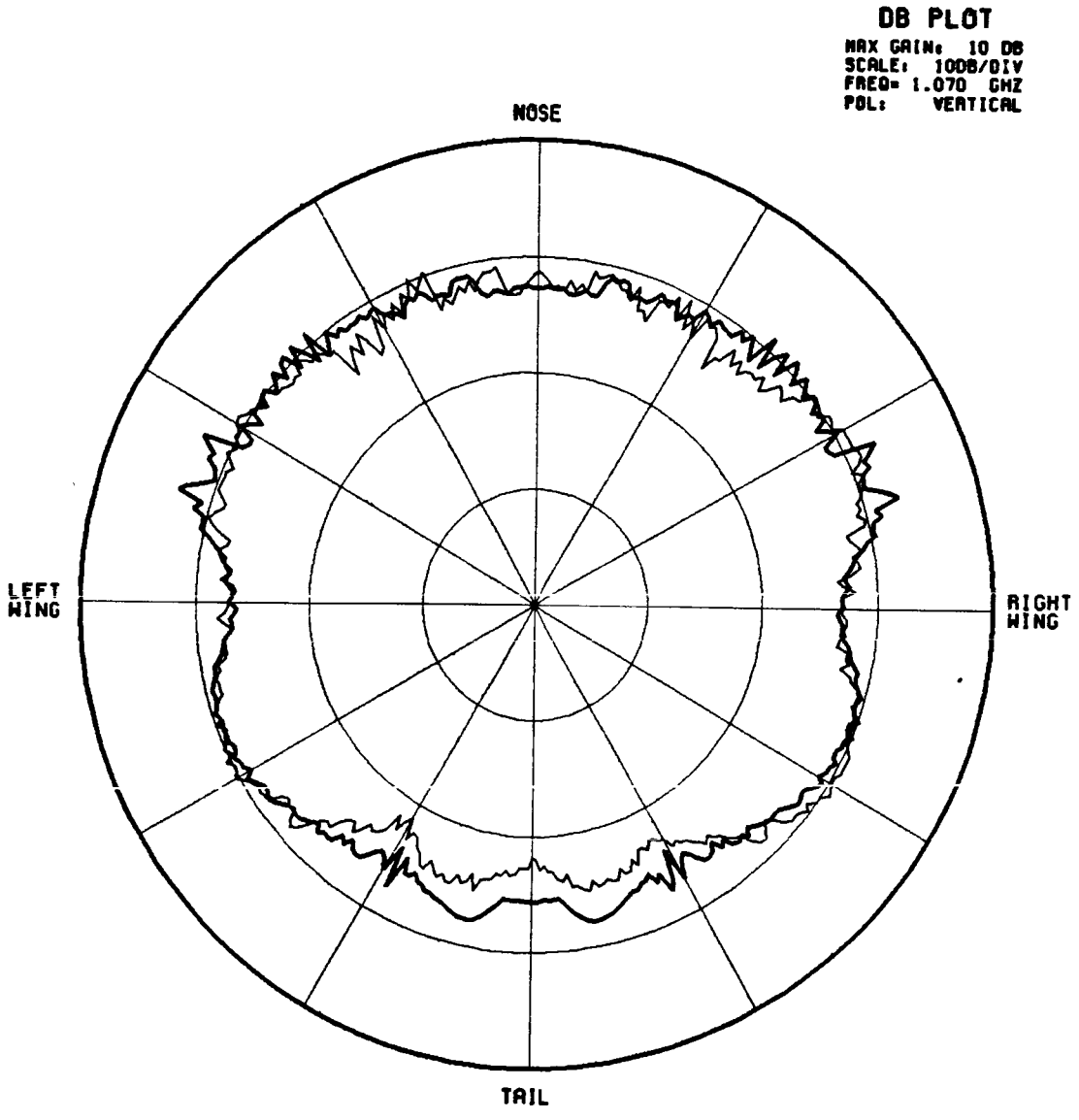

Figure 3.9. P-3B azimuth L-band antenna radiation pattern.
——— Calculated (including 2nd source)
——— Measured

at modelling the physical blockage. The blockage caused by the beacon, or by any object near a source, is a problem which could be further investigated. The problem is that when the beacon was modelled by a plate in the Airborne Antenna Code, the code could not model any coupling effects. Also, the plate was too close to the source so the code calculated a large null in the rear quadrant. The beacon was therefore modelled as a shorted dipole so that the coupling effect could be included in the Airborne Antenna Code as a monopole. The Airborne Antenna Code input file for this simulation is shown in Figure 3.10. The input file for the single source problem was the same except for the SP: and the second SG: and EX: commands.

The elevation pattern for the P-3B L-band antenna was available, so it was also calculated. Results are presented in Figures 3.11 and 3.12. Figure 3.11 shows the calculated single source results compared to the measured results and shows good agreement off the nose and a difference of 1-3 dB off the tail. The second source was included for Figure 3.12 which shows even better agreement.

In the case of the P-3B L-band antenna, the Airborne Antenna Code and the ESP code proved to be valuable tools for simulating the antenna performance. In both azimuth and elevation patterns, agreement between measured and calculated results was very good.

```
UN:  IN INCHES
3
FG:  P-3B FUSELAGE GEOMETRY AT STATION 352
71.0,71.0,548.0,1136.0
F
0.,0.,0.
FC:  TRUNCATE NOSE & TAIL
F,F
524.0,-548.
FQ:  FREQUENCY
1,1.070,1.0
SG:  SOURCE GEOMETRY
0.,0.0
1
0.,0.
0.,0.,0.,2.76,3
1.,0.
PG:  PORT WING
4,T
34.,-56.,-4.
0.,-598.,-103.
0.,-598.,-198.
34.,-56.,-215.
PG:  STARBOARD WING
4,T
34.,56.,-215.
0.,598.,-198.
0.,598.,-103.
34.,56.,-4.
PG:  PORT TAIL WING
4,T
0.,-37.,524.
-14.,-246.,506.
-14.,-246.,453.
0.,-37.,383.
PG:  STARBOARD TAIL WING
4,T
0.,37.,383.
-14.,246.,453.
-14.,246.,506.
0.,37.,524.
PG:  DOPPLER BLOCKAGE
4,T
68.,16.,172.
76.,16.,172.
76.,-16.,172.
68.,-16.,172.
```

Figure 3.10. Airborne antenna code input file for P-3B L-band antenna simulation.

```
PG:  INSIDE INNER STARBOARD ENGINE HOUSING
3,F
22.,150.,-76.
22.,150.,-204.
62.,150.,-204.
PG:  OUTSIDE INNER STARBOARD ENGINE HOUSING
3,F
19.,202.,-76.
59.,202.,-204.
19.,202.,-204.
PG:  BOTTOM INNER STARBOARD ENGINE HOUSING
4,F
62.,150.,-204.
59.,202.,-204.
19.,202.,-76.
22.,150.,-76.
PG:  INSIDE INNER PORT ENGINE HOUSING
3,F
22.,-150.,-76.
62.,-150.,-204.
22.,-150.,-204.
PG:  OUTSIDE INNER PORT ENGINE HOUSING
3,F
19.,-202.,-76.
19.,-202.,-204.
59.,-202.,-204.
PG:  BOTTOM INNER PORT ENGINE HOUSING
4,F
59.,-202.,-204.
62.,-150.,-204.
22.,-150.,-76.
19.,-202.,-76.
PG:  INSIDE OUTER STARBOARD ENGINE HOUSING
3,F
11.,317.,-100.
11.,317.,-199.
40.,317.,-199.
PG:  OUTSIDE OUTER STARBOARD ENGINE HOUSING
3,F
8.,368.,-100.
37.,368.,-199.
8.,368.,-199.
PG:  BOTTOM OUTER STARBOARD ENGINE HOUSING
4,F
40.,317.,-199.
37.,368.,-199.
8.,368.,-100.
11.,317.,-100.
68.,-16.,172.
```

Figure 3.10. (continued).

```
PG:  INSIDE OUTER PORT ENGINE HOUSING
3,F
11.,-317.,-100.
40.,-317.,-199.
11.,-317.,-199.
PG:  OUTSIDE OUTER PORT ENGINE HOUSING
3,F
8.,-368.,-100.
8.,-368.,-199.
37.,-368.,-199.
PG:  BOTTOM OUTER PORT ENGINE HOUSING
4,F
37.,-368.,-199.
40.,-317.,-199.
11.,-317.,-100.
8.,-368.,-100.
BO:  BINARY OUTPUT
T
PD:  ELEVATION PATTERN
90.,90.,89.
0,360,1
T,0.0
SP:  SUPERIMPOSE SOURCES
T,1.0,0.0
EX:  EXECUTE
SG:  2ND SOURCE
0.0,11.0
1
0.0,0.0
0.0,0.0,0.0,2.76,3
0.237,-125.0
EX:  EXECUTE
```

Figure 3.10. (continued).

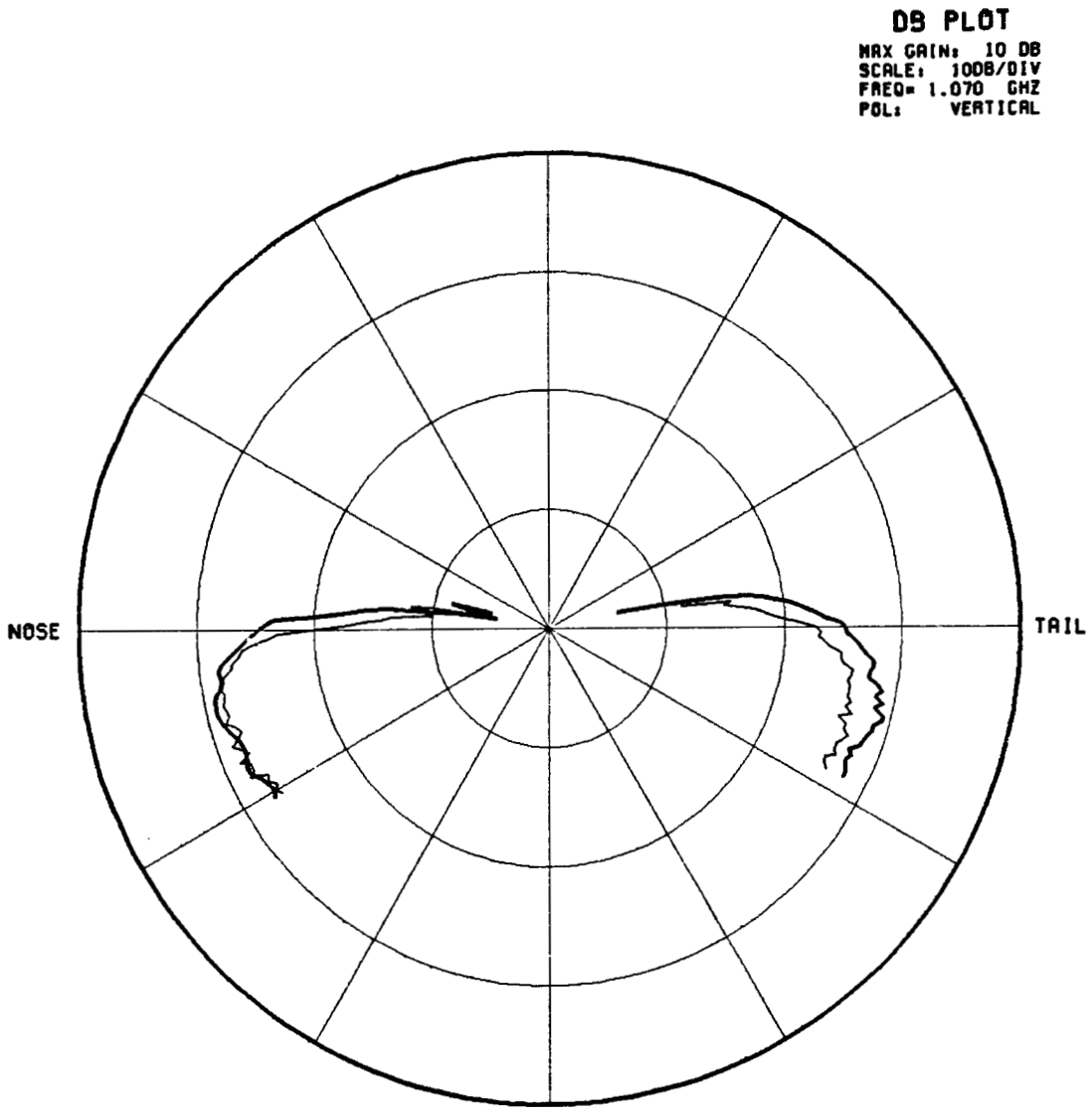

Figure 3.11. P-3B elevation L-band antenna radiation pattern.
——— Calcualted (using single source)
——— Measured

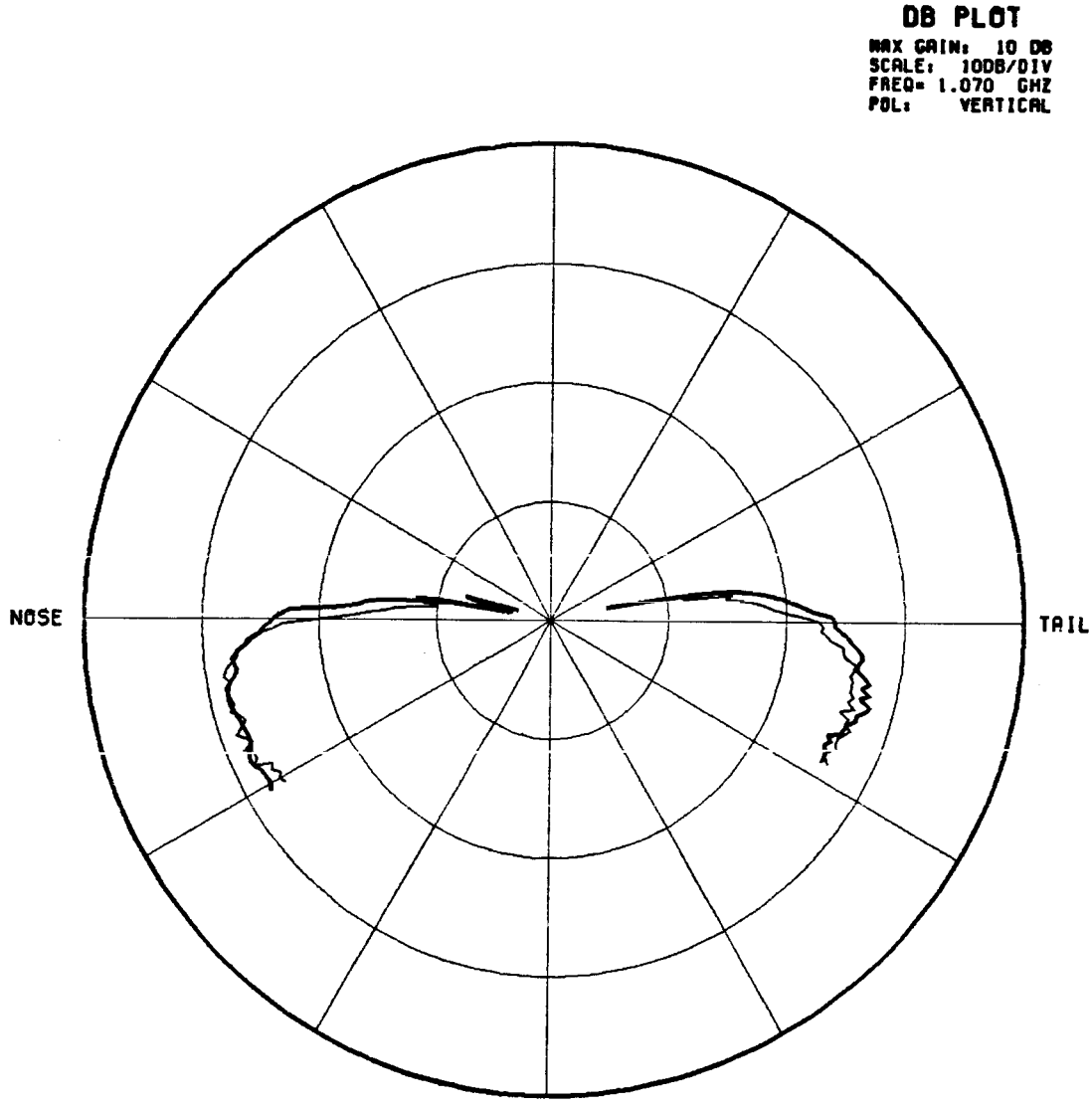

Figure 3.12. P-3B elevation L-band antenna radiation pattern.
——— Calculated (including second source)
——— Measured

CHAPTER IV

A-7E UHF RELAY POD ANALYSIS

In this chapter a UHF relay pod installed on an A-7E is analyzed using the Airborne Antenna and ESP Codes. The A-7E is a subsonic single-seat tactical fighter as shown in Figure 4.1. The relay pod is a 15 foot equipment pod mounted on the outer port underwing pylon. The pod is equipped with various receiver/transmitters and four UHF blade antennas. The pod and antenna locations are illustrated in Figure 4.2. An omnidirectional radiation pattern in the azimuth plane is desired for each antenna. The forward-most antenna is analyzed in this chapter. Figure 4.3 shows the measured radiation pattern which has blockage and nulls throughout the pattern. The measured results were taken in flight at the Naval Air Test Center (Patuxent River, Maryland).

In the analysis of the A-7E UHF relay pod, the ESP code was first used to determine the currents induced on each antenna on the pod. The four antennas were modelled as half-wavelength dipoles in free-space, as shown in Figure 4.4, using the ESP input file shown in Figure 4.5. The forward-most antenna was excited with a unit amplitude source, and the three rear antennas were loaded with 50 ohms to simulate their connections to 50-ohm cables. A partial listing of the ESP code results

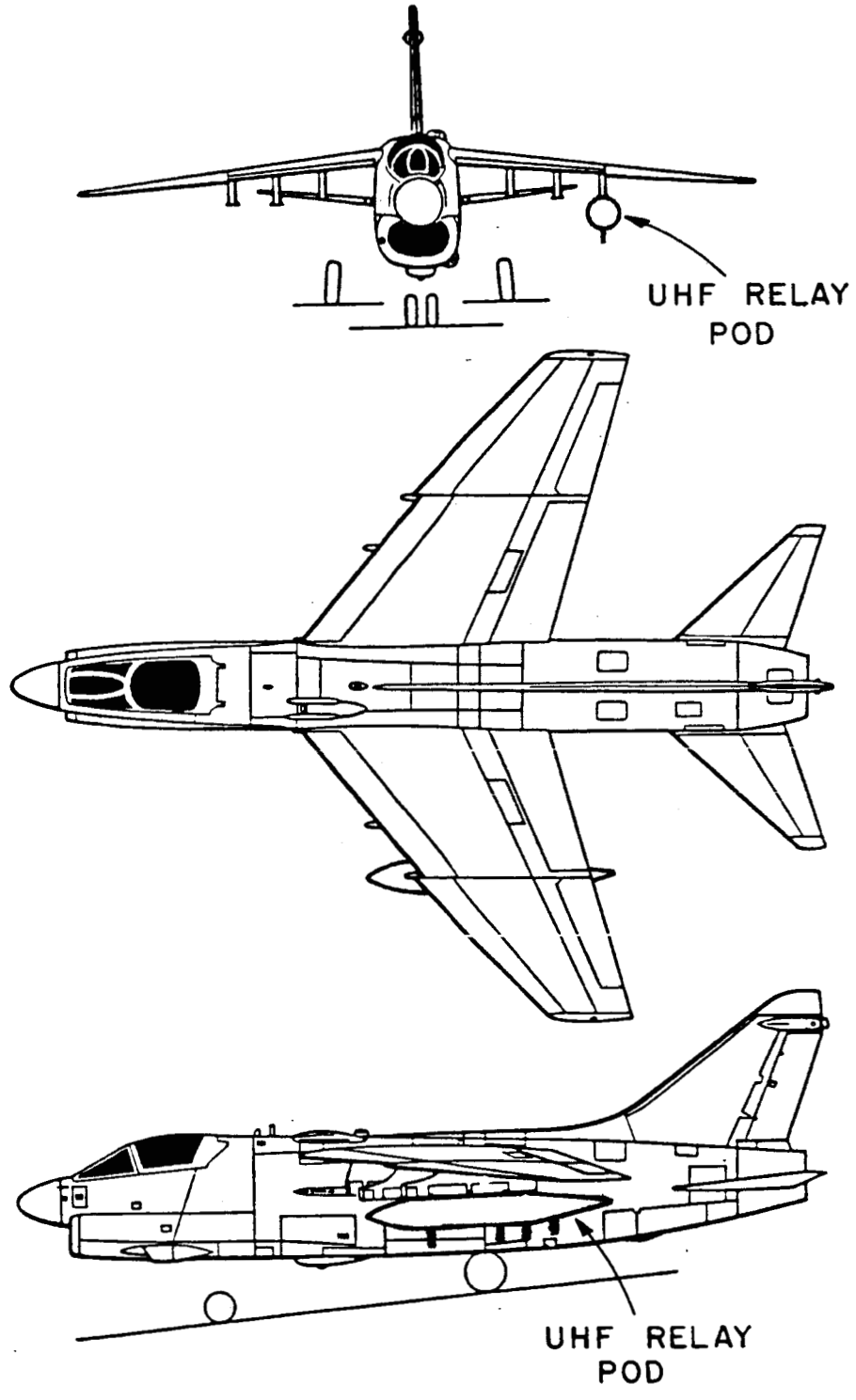

Figure 4.1. A-7E line drawing.

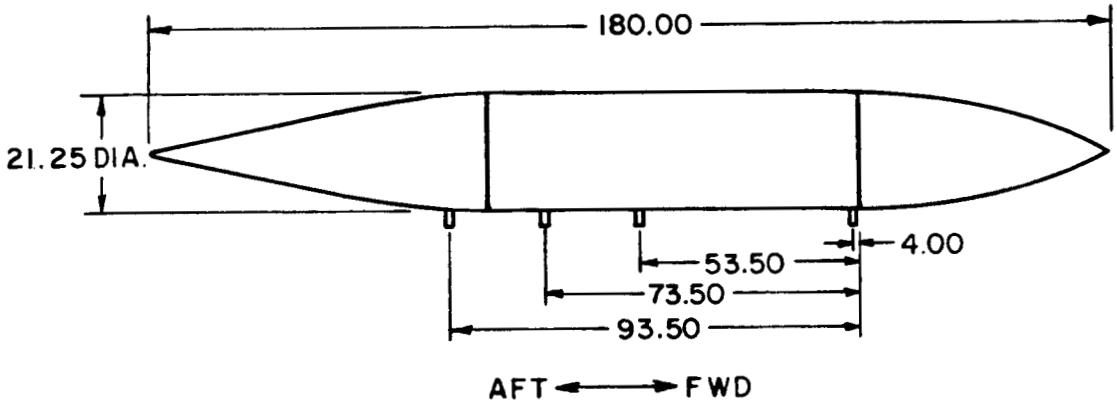

Figure 4.2. UHF relay pod.

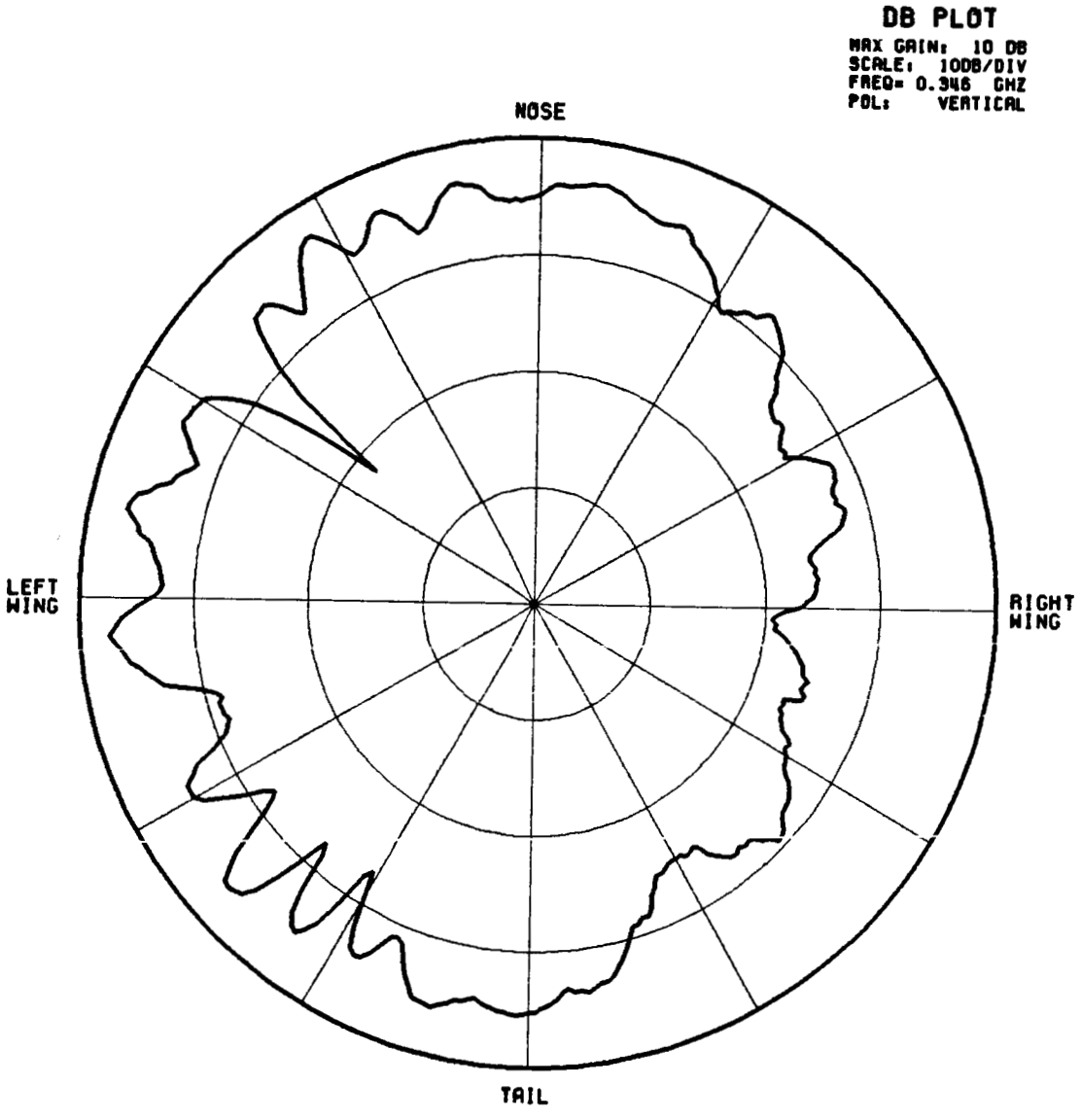

Figure 4.3. Measured A-7E UHF relay pod azimuth antenna radiation pattern.

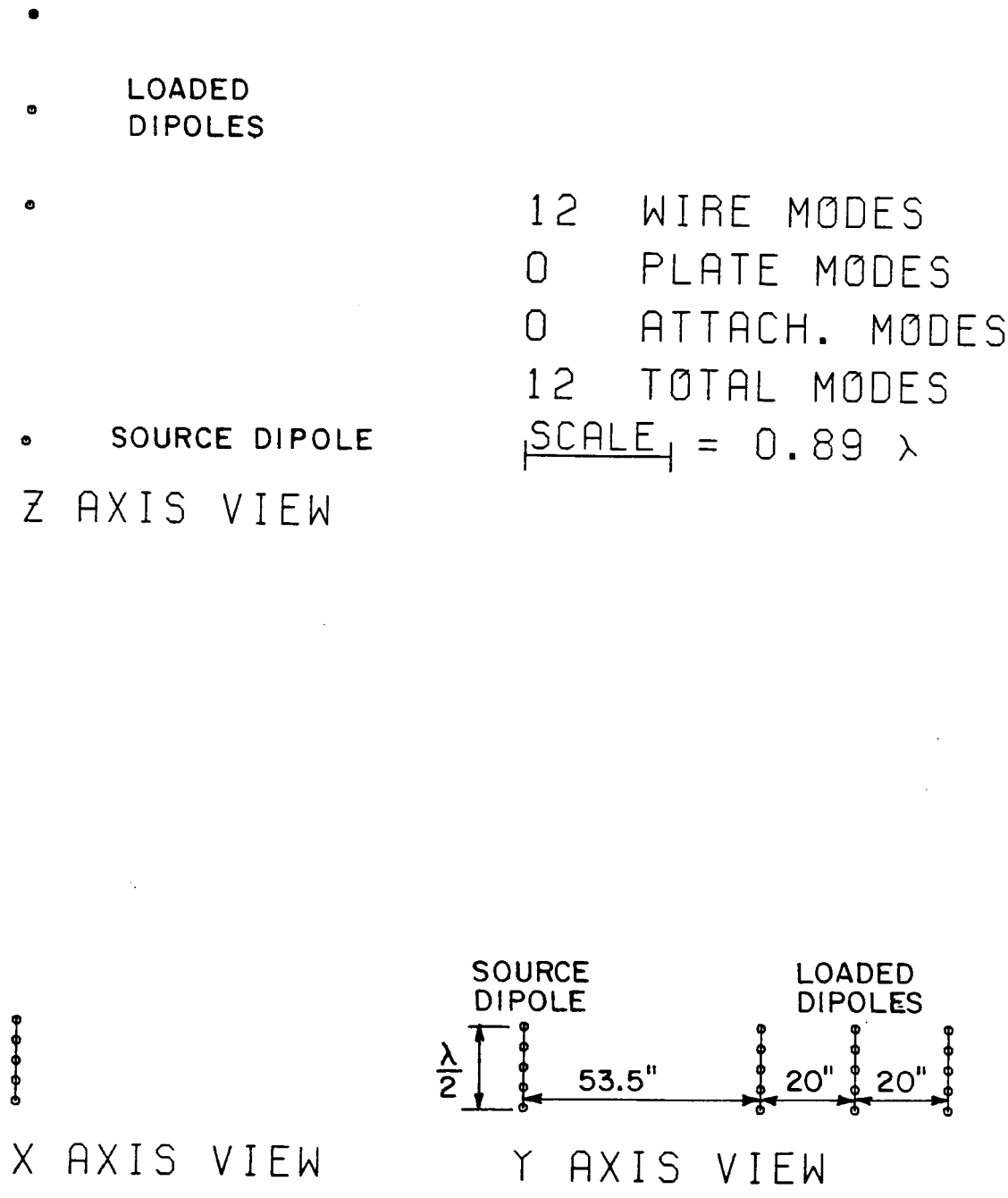

Figure 4.4. Antenna geometry for ESP code.

```
0  2  1  1  1  0  4  10  18  1  1
0  0  1  0.0
1  0  1  95.0
0  0  1  0.0  0.0  0.0
0  0  1  0.0
346.1  -1  0.0005
0  0
0  0
16  20  0  1
0.0  0.0  -0.2166          !TEST MONOPOLE
0.0  0.0  -0.1083
0.0  0.0  +0.0000
0.0  0.0  +0.1083
0.0  0.0  +0.2166
-1.2573  0.0  -0.2166              !MONOPOLE 49.5 INCHES
-1.2573  0.0  -0.1083              !BEHIND TEST MONOPOLE
-1.2573  0.0  +0.0000
-1.2573  0.0  +0.1083
-1.2573  0.0  +0.2166
-1.7653  0.0  -0.2166              !MONOPOLE 69.5 INCHES
-1.7653  0.0  -0.1083              !BEHIND TEST MONOPOLE
-1.7653  0.0  +0.0000
-1.7653  0.0  +0.1083
-1.7653  0.0  +0.2166
-2.2733  0.0  -0.2166              !MONOPOLE 89.5 INCHES
-2.2733  0.0  -0.1083              !BEHIND TEST MONOPOLE
-2.2733  0.0  +0.0000
-2.2733  0.0  +0.1083
-2.2733  0.0  +0.2166
1   2
2   3
3   4
4   5
6   7
7   8
8   9
9   10
11  12
12  13
13  14
14  15
16  17
17  18
18  19
19  20
3  0  (1.0,0.0)  (0.0,0.0)
```

Figure 4.5. ESP input file.

is given in Figure 4.6. The relative currents induced on each dipole are indicated in the boxes on page 42. Modes 2, 5, 8 and 11 are the center modes of each dipole. The currents of modes 5, 8, and 11, relative to the current of mode 2 are input into the Airborne Antenna Code as additional sources.

In the Airborne Antenna Code, the ellipsoid is used to model the pod, rather than the aircraft fuselage. The code was first run without any additional plates to determine the effects of the three rear antennas. The Airborne Antenna Code input file for this geometry is shown in Figure 4.7, and the calculated radiation pattern is shown in Figure 4.8. These results show minimal interference compared to the measured pattern.

Eight plates were added to the ellipsoid to simulate the side of the aircraft, the wing, the horizontal stabilizer, and the pod mount. This geometry is illustrated in Figure 4.9, using the input file shown in Figure 4.10. It should be noted that the diameter of the pod was 0.6227 wavelengths which may be pushing the accuracy of the code, but the calculated pattern shown in Figure 4.11 does very well to show the lobing and blockage caused by the side of the aircraft.

This is a case where the Airborne Antenna Code could have been used in the early stages of development to show the interference caused by the aircraft. The Airborne Antenna Code used a simple input geometry to predict a fairly complicated radiation pattern, and even though the diameter of the ellipsoid was less than a wavelength, the code provided reasonably good results.

INPUT DATA

FREQ.(MHZ) = 346.100
WAVE(M) = 0.867

WIRE RADIUS(M) = 0.0005000

WIRE CONDUCTIVITY = -1.00 MEGAMHOS/M

GEOMETRY FOR THE 0 PLATES

20 POINTS ON THE WIRE

I	X (I)	Y (I)	Z (I)
1	0.0000E+00	0.0000E+00	-0.2166E+00
2	0.0000E+00	0.0000E+00	-0.1083E+00
3	0.0000E+00	0.0000E+00	0.0000E+00
4	0.0000E+00	0.0000E+00	0.1083E+00
5	0.0000E+00	0.0000E+00	0.2166E+00
6	-0.1257E+01	0.0000E+00	-0.2166E+00
7	-0.1257E+01	0.0000E+00	-0.1083E+00
8	-0.1257E+01	0.0000E+00	0.0000E+00
9	-0.1257E+01	0.0000E+00	0.1083E+00
10	-0.1257E+01	0.0000E+00	0.2166E+00
11	-0.1765E+01	0.0000E+00	-0.2166E+00
12	-0.1765E+01	0.0000E+00	-0.1083E+00
13	-0.1765E+01	0.0000E+00	0.0000E+00
14	-0.1765E+01	0.0000E+00	0.1083E+00
15	-0.1765E+01	0.0000E+00	0.2166E+00
16	-0.2273E+01	0.0000E+00	-0.2166E+00
17	-0.2273E+01	0.0000E+00	-0.1083E+00
18	-0.2273E+01	0.0000E+00	0.0000E+00
19	-0.2273E+01	0.0000E+00	0.1083E+00
20	-0.2273E+01	0.0000E+00	0.2166E+00

MODES ON THE WIRE STRUCTURE

MAXIMUM NUMBER OF MODES AT ONE POINT = 2
MINIMUM NUMBER OF MODES AT ONE POINT = 1
NUMBER OF WIRE MODES = 12

I	I1(I)	I2(I)	I3(I)	JA(I)	JB(I)
1	1	2	3	1	2
2	2	3	4	2	3
3	3	4	5	3	4
4	6	7	8	5	6
5	7	8	9	6	7
6	8	9	10	7	8
7	11	12	13	9	10
8	12	13	14	10	11
9	13	14	15	11	12
10	16	17	18	13	14
11	17	18	19	14	15
12	18	19	20	15	16

Figure 4.6. Partial listing of ESP results.

```
 16 SEGMENTS ON THE WIRE
 J     IA(J)    IB(J)     D(J)(M)

 1       1        2      0.10830E+00
 2       2        3      0.10830E+00
 3       3        4      0.10830E+00
 4       4        5      0.10830E+00
 5       6        7      0.10830E+00
 6       7        8      0.10830E+00
 7       8        9      0.10830E+00
 8       9       10      0.10830E+00
 9      11       12      0.10830E+00
10      12       13      0.10830E+00
11      13       14      0.10830E+00
12      14       15      0.10830E+00
13      16       17      0.10830E+00
14      17       18      0.10830E+00
15      18       19      0.10830E+00
16      19       20      0.10830E+00


 LISTING OF LOADS AND GENERATORS

  0.1000E+01    0.0000E+00 VOLTS BY PT. A OF SEGMENT   3
  0.5000E+02    0.0000E+00 OHMS BY PT. A OF SEGMENT   7
  0.5000E+02    0.0000E+00 OHMS BY PT. A OF SEGMENT  11
  0.5000E+02    0.0000E+00 OHMS BY PT. A OF SEGMENT  15

 NWR = NUMBER OF WIRE MODES =   12
 NPLTM = NUMBER OF PLATE MODES =    0
 NAT = NUMBER OF ATTACHMENT MODES =    0


  ANTENNA MODAL CURRENTS
MODE   REL MAG      ABS MAG      PHASE        III COMPLEX III

  1     0.765     0.0084501      -31.      0.007211     -0.004406
  2     1.000     0.0110438      -27.      0.009883     -0.004928
  3     0.765     0.0084501      -31.      0.007211     -0.004406
  4     0.067     0.0007370       58.      0.000386      0.000628
  5     0.091     0.0010077       55.      0.000578      0.000825
  6     0.067     0.0007370       58.      0.000386      0.000628
  7     0.040     0.0004422     -168.     -0.000433     -0.000090
  8     0.055     0.0006058     -172.     -0.000599     -0.000088
  9     0.040     0.0004422     -168.     -0.000433     -0.000090
 10     0.034     0.0003757      -28.      0.000332     -0.000176
 11     0.047     0.0005147      -31.      0.000440     -0.000268
 12     0.034     0.0003757      -28.      0.000332     -0.000176

INPUT ADMITTANCE(MHOS) =    0.009883 J  -0.004928
INPUT IMPEDANCE(OHMS) =     81.034 J     40.406
EFFICIENCY(PERCENT) =  99.167
```

Figure 4.6. (continued).

```
UN:  UNITS IN INCHES
3
FG:  POD GEOMETRY
10.6,10.6,48.0,132.0
T
0.,0.,0.
FQ:  FREQUENCY
1,0.3461,1.0
SG:  SOURCE GEOMETRY
0.0,0.0
1
0.,0.
0.,0.,0.,8.53,3
1.,0.
BO:  BINARY OUTPUT
T
PD:  AZIMUTH PATTERN
90.,0.,87.
0,360,1
T,0.0
SP:SUPERIMPOSE SOURCES
T,1.0,0.0
EX:EXECUTE
SG:  2ND SOURCE
0.0,-49.5
1
0.,0.
0.,0.,0.,8.53,3
0.091,82.0
EX:  EXECUTE
SG:  3RD SOURCE
0.0,-69.5
1
0.,0.
0.,0.,0.,8.53,3
0.055,-145.0
EX:  EXECUTE
SG:  4TH SOURCE
0.0,-89.5
1
0.,0.
0.,0.,0.,8.53,3
0.047,-4.0
EX:  EXECUTE
```

Figure 4.7. Airborne antenna code input file.

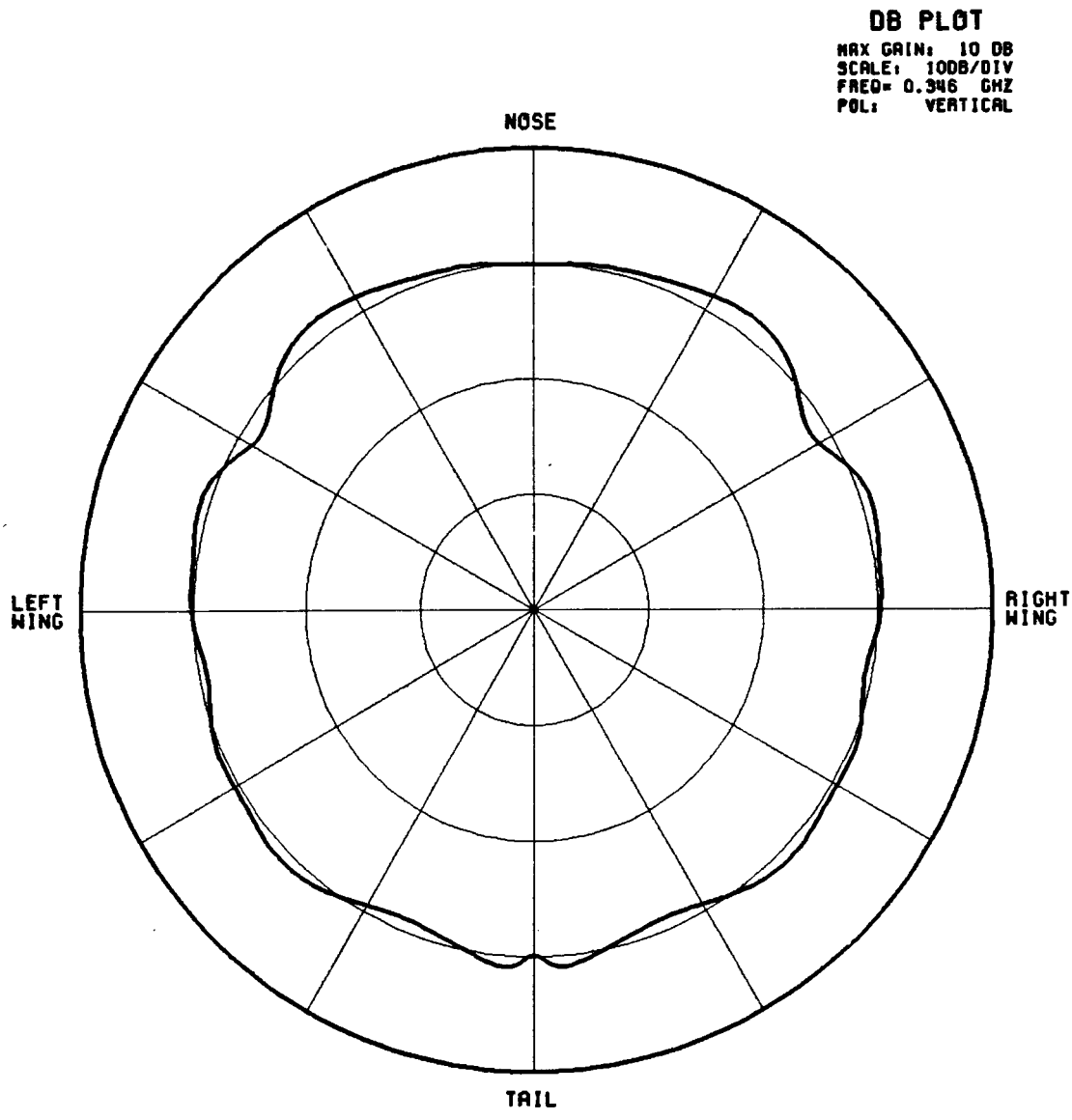

Figure 4.8. Azimuth antenna radiation pattern of the monopole on the ellipsoid with the three rear monopole present.

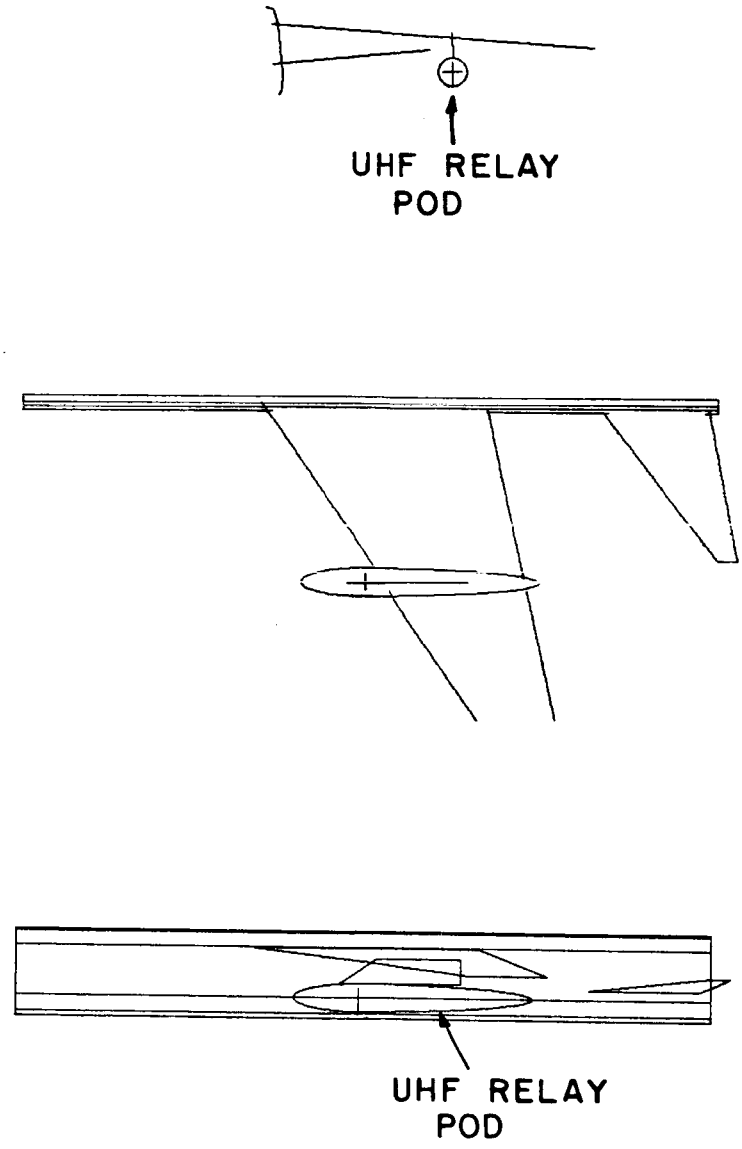

Figure 4.9. Computer model of A-7E UHF relay pod.

```
UN:IN INCHES
3
FG:POD GEOMETRY
10.6,10.6,48.0,132.0
T
0.,0.,0.
FQ:FREQUENCY
1,0.3461,1.0
SG:SOURCE GEOMETRY
0.0,0.0
1
0.,0.
0.,0.,0.,8.53,3
1.,0.
PG:POD MOUNT
4,F
-10.7,0.5,13.3
-29.6,0.,-14.6
-29.6,0.,-79.2
-10.7,0.5,-79.2
PG:WING
4,F
-17.4,105.4,-86.0
-17.4,105.4,-143.8
-36.8,-135.6,-92.8
-36.8,-135.6,77.2
PG:SIDE OF A/C
4,F
-48.8,-135.0,-265.0
-48.8,-135.0,255.0
-49.8,-140.0,255.0
-49.8,-140.0,-265.0
PG:
4,F
-48.8,-135.0,-265.0
-48.8,-135.0,255.0
-37.8,-132.0,255.0
-37.8,-132.0,-265.0
PG:
4,F
-37.8,-132.0,-265.0
-37.8,-132.0,255.0
0.0,-129.0,255.0
0.0,-129.0,-265.0
PG:
4,F
0.0,-129.0,-265.0
0.0,-129.0,255.0
12.0,-130.0,255.0
12.0,-130.0,-265.0
PG:
4,F
12.0,-130.0,-265.0
12.0,-130.0,255.0
16.0,-132.0,255.0
16.0,-132.0,-265.0
PG:TAIL WING
4,F
-7.2,-135.6,-175.0
-7.2,-135.6,-257.5
-17.4,-17.0,-280.0
-17.4,-17.0,-265.0
BO:BINARY OUTPUT
T
PD:AZIMUTH PLANE PATTERN
90.,0.,86.
0,360,1
T,0.0
SP:SUPERIMPOSE OTHER SOURCES
T,1.0,0.0
EX:EXECUTE
SG:HI SOURCE
0.0,-49.5
1
0.,0.
0.,0.,0.,8.53,3
0.091,82.0
EX:EXECUTE
SG:MID SOURCE
0.0,-69.5
1
0.,0.
0.,0.,0.,8.53,3
0.055,-145.0
EX:EXECUTE
SG:LO SOURCE
0.0,-89.5
1
0.,0.
0.,0.,0.,8.53,3
0.047,-4.0
EX:EXECUTE
```

Figure 4.10. Airborne antenna input file for goemetry of Figure 4.9.

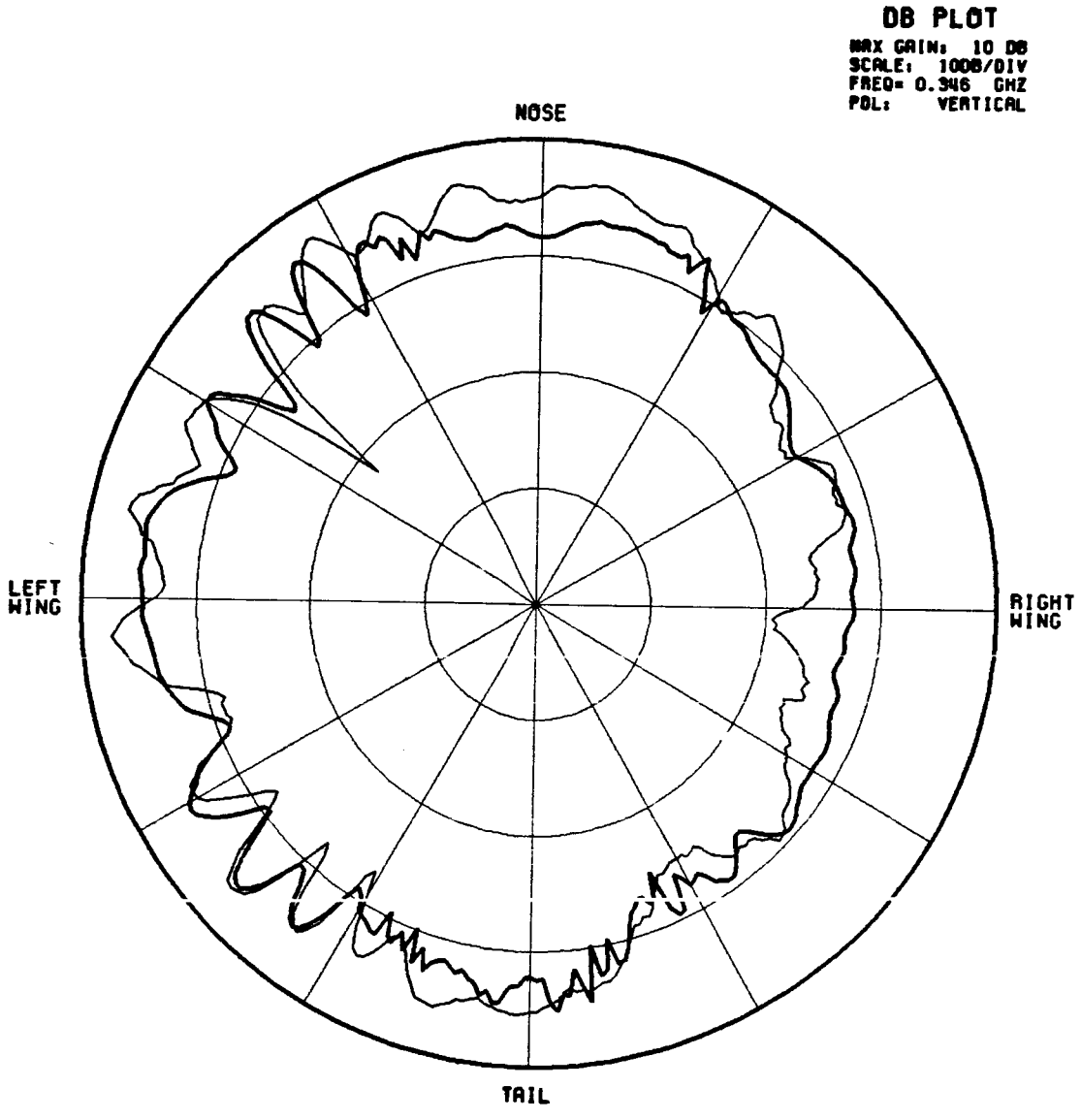

Figure 4.11. A-7E UHF relay pod azimuth antenna radiation pattern.
——— Calculated
——— Measured

CHAPTER V

TRAFFIC ALERT AND COLLISION AVOIDANCE SYSTEM ANALYSIS

The Basic Scattering Code (BSC) is used in this chapter to analyze the Traffic Alert and Collision Avoidance System (TCAS) as installed on a Bell Long Ranger helicopter. The Long Ranger helicopter is a turbine-powered general-purpose seven-seat light helicopter. TCAS is a traffic advisory system which informs the pilot of the angle-of-arrival (AOA) of an incoming signal, and therefore, the bearing in azimuth of another aircraft in the vicinity. The system utilizes a four-element array of quarter-wave monopoles, each positioned on the corners of a quarter-wavelength square as shown in Figure 5.1(a). The array is located on a flat area above the cockpit, in front of the rotor shaft as shown in Figure 5.1(b). The outputs from each antenna are processed through a network of hybrids. This network has two outputs; a sum and delta output. The output of the sum channel is the four input signals added in phase. The output of the delta channel is a sum of the four inputs with different phase shifts added to three of the inputs. The sum and delta output are, respectively given algebraically by

$$\Sigma = A + B + C + D \tag{5.1}$$

and

$$\Delta = (D-B) + j(C-A) \tag{5.2}$$

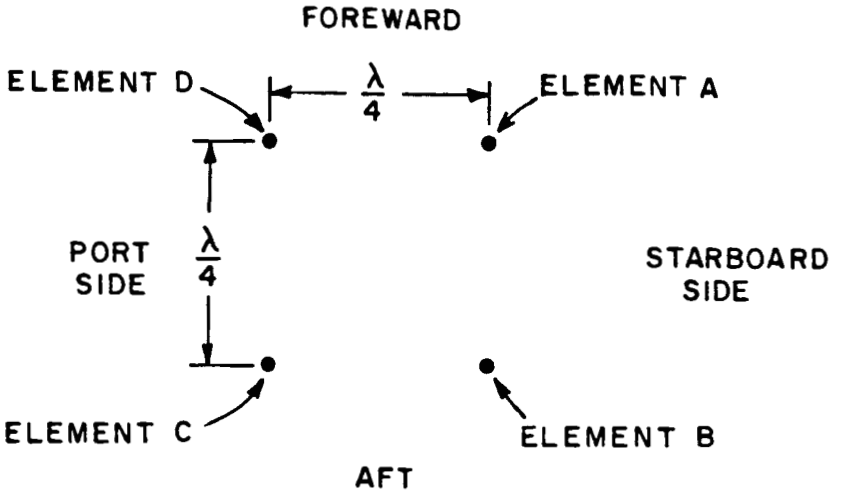

(a) ARRAY GEOMETRY

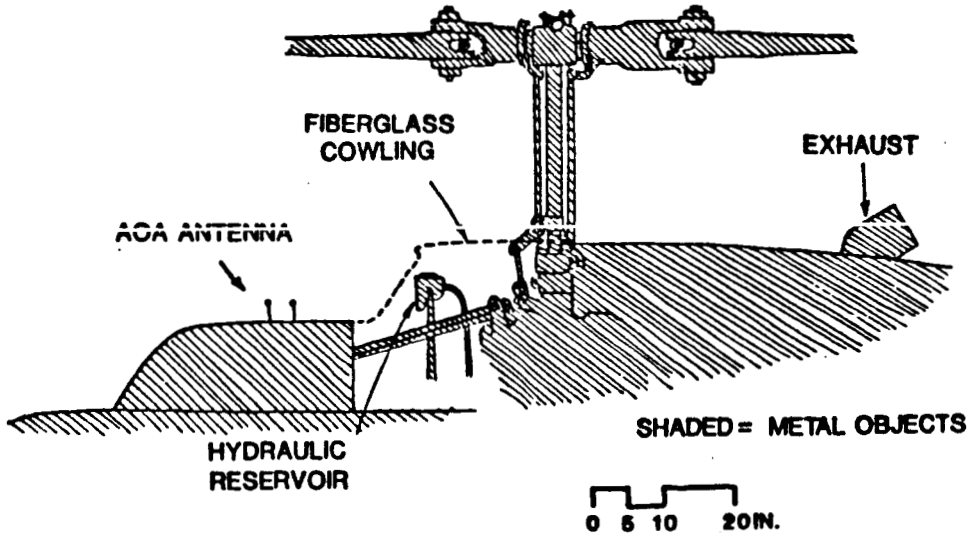

(b) ARRAY LOCATION

Figure 5.1. AOA array geometry and location.

where A, B, C and D represent the complex voltage levels of the four AOA antennas. The angle-of-arrival is then given by

$$\theta_A = \phi_\Delta - \phi_\Sigma - \xi \tag{5.3}$$

where θ_A is the angle-of-arrival, ϕ_Σ is the phase of the sum channel, ϕ_Δ is the phase of the delta channel and ξ is a constant offset angle determined through calibration.

Measured data has been taken on the TCAS antenna by the Lincoln Laboratory of the Massachusetts Institute of Technology. A signal was radiated toward the aircraft as it hovered just above the ground. As the aircraft slowly rotated, the actual bearing of the transmitter and the TCAS output heading were recorded. Results are shown in Figure 5.2.

Measurements of the AOA antenna system were also taken in an anechoic chamber. The four monopoles were mounted on an aluminum circular ground plane, 4 feet in diameter, and rotated in the presence of a test signal. The plot of the output phase versus actual bearing for this test condition is called the AOA transfer function. This transfer function, shown in Figure 5.3, indicates the phase difference between the sum and delta channels versus the incident bearing angle.

Three metal cylinders were placed near the antenna to simulate the rotor shaft. The cylinders were mounted on a turntable as shown in Figure 5.4, and the results of this configuration are shown in Figure 5.5.

To simulate the problem on the computer, the ESP code was first used ot determine any coupling effects. As a backscatter problem, the monopoles were modelled as dipoles in free-space, and the ESP code calculated the currents induced on each dipole as the angle-of-arrival

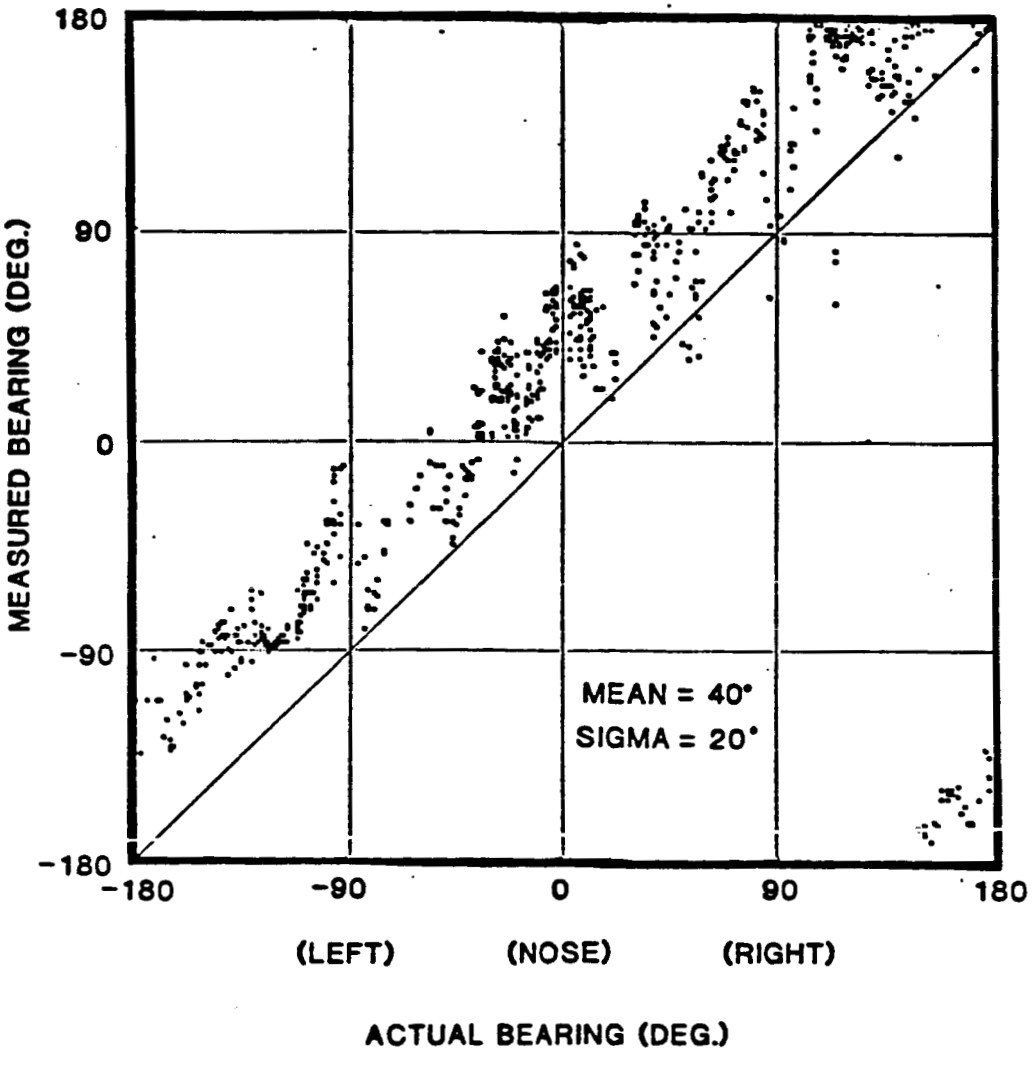

Figure 5.2. AOA antenna performance hovering just above the ground.

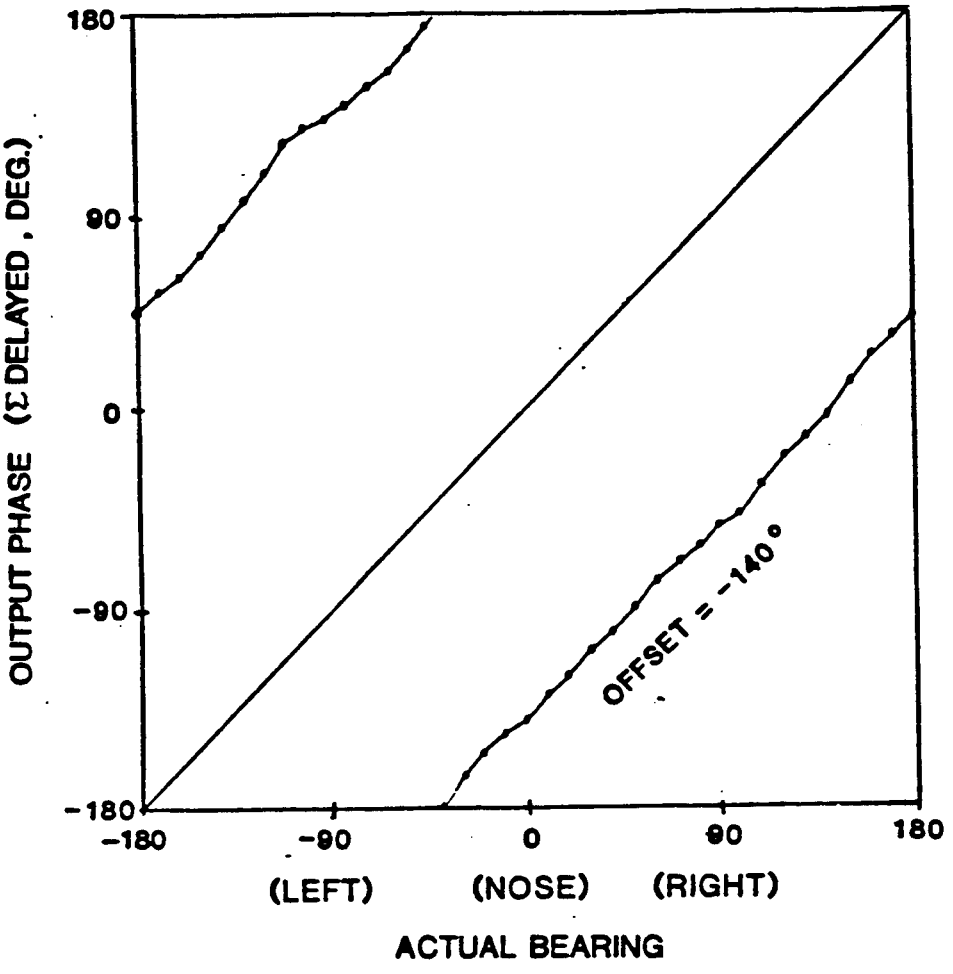

Figure 5.3. AOA performance of antenna on a groundplane.

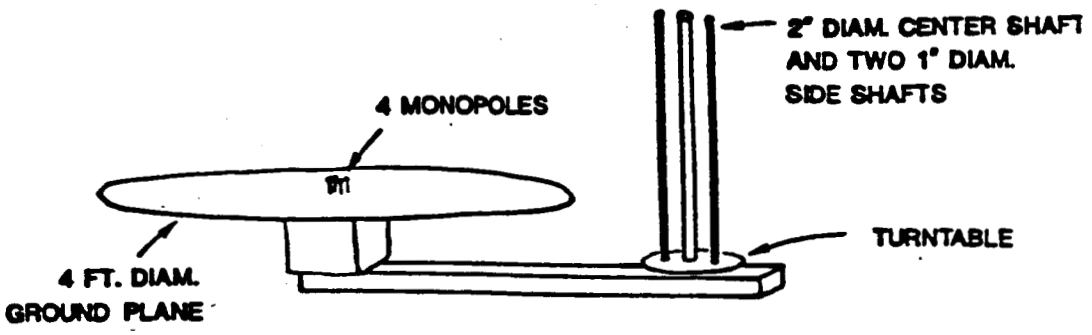

Figure 5.4. AOA antenna mounted near rotating cylinders.

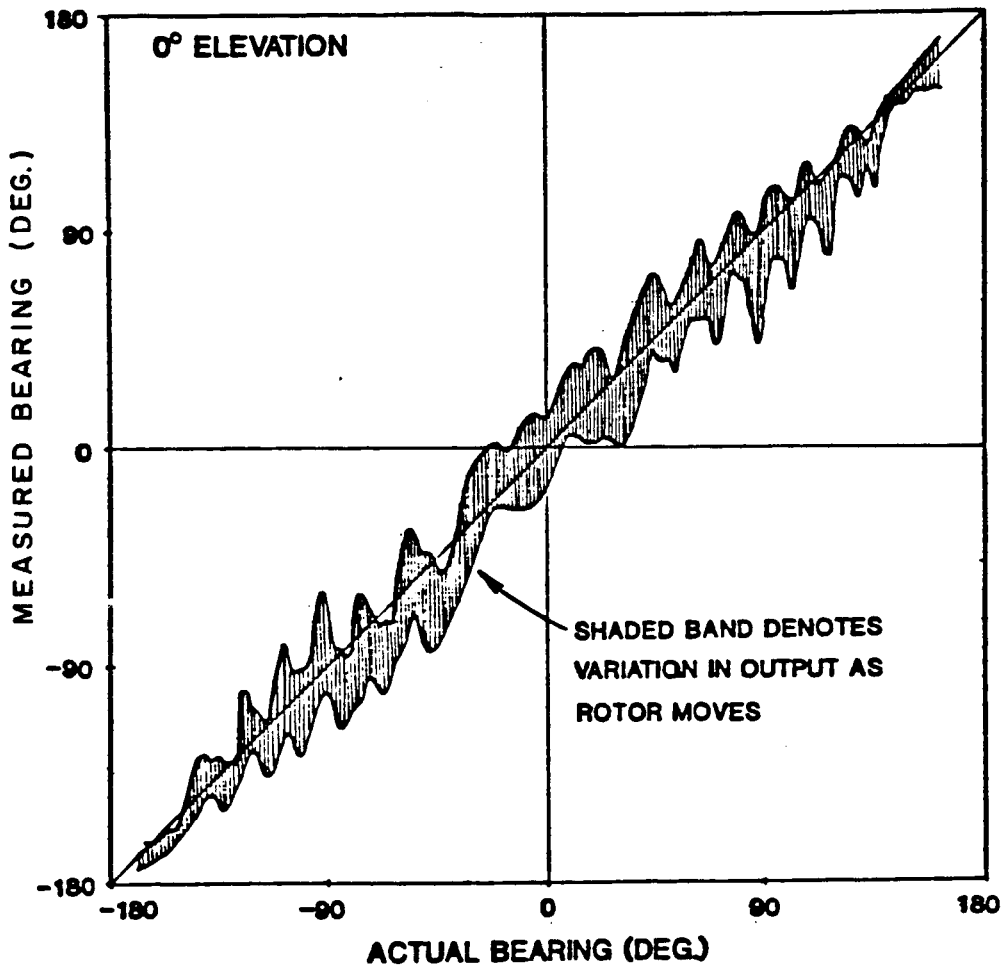

Figure 5.5. AOA performance of antenna near rotating cylinders.

of the incident field varied. The ESP input file and the geometry are shown in Figures 5.6 and 5.7, respectively. The calculated currents were then added using Equations (5.1) and (5.2) to determine the AOA transfer function. The results are shown in Figure 5.8 with an offset of 5.38 degrees included in the results. The results show very little interference from coupling.

The BSC was also used to calculate the transfer function using the same geometry in Figure 5.7. The field patterns of each dipole was calculated individually and the four fields were used in Equations (5.1) and (5.2) to produce a sum and delta output. The phase of these two fields were compared, and the difference is the transfer function shown in Figure 5.9. These results also show very little interference and are nearly identical to Figure 5.8. This suggests that the small amount of fluctuation is because the geometry looks symmetrical from eight aspect angle. The offset here was 45 degrees, which will be constant in the following BSC applications.

Three cylinders were added to the model as shown in Figure 5.10. The BSC calculated the fields for the geometry shown and with the cylinders rotated about the center cylinder's axis to simulate the anechoic chamber results. Four calculations were made; the geometry shown and with the cylinders rotated counter-clockwise 45, 90 and 135 degrees. The results are overlayed in Figure 5.11 to simulate the phase variation as the rotor shaft turns. This figure now shows the interference experienced in the anechoic chamber.

```
1  2  1  1  0  0  4  10  18  1  1
0  0  1  0.0
0  0  1  0.0
0  0  1  0.0  0.0  0.0
1  0  1.0  90.0
1090.0  -1  0.00025
0  0
0  0
16  20  0  4
0.0344   0.0344   -.0688    !MONOPOLE A
0.0344   0.0344   -.0344
0.0344   0.0344   0.0
0.0344   0.0344   +.0344
0.0344   0.0344   +.0688
-.0344   0.0344   -.0688    !MONOPOLE B
-.0344   0.0344   -.0344
-.0344   0.0344   0.0
-.0344   0.0344   +.0344
-.0344   0.0344   +.0688
-.0344   -.0344   -.0688    !MONOPOLE C
-.0344   -.0344   -.0344
-.0344   -.0344   0.0
-.0344   -.0344   +.0344
-.0344   -.0344   +.0688
0.0344   -.0344   -.0688    !MONOPOLE D
0.0344   -.0344   -.0344
0.0344   -.0344   0.0
0.0344   -.0344   +.0344
0.0344   -.0344   +.0688
1   2
2   3
3   4
4   5
6   7
7   8
8   9
9   10
11  12
12  13
13  14
14  15
16  17
17  18
18  19
19  20
 3  0  (0.0,0.0)  (50.0,0.0)
 7  0  (0.0,0.0)  (50.0,0.0)
11  0  (0.0,0.0)  (50.0,0.0)
15  0  (0.0,0.0)  (50.0,0.0)
```

Figure 5.6. ESP input file for AOA antenna simulation.

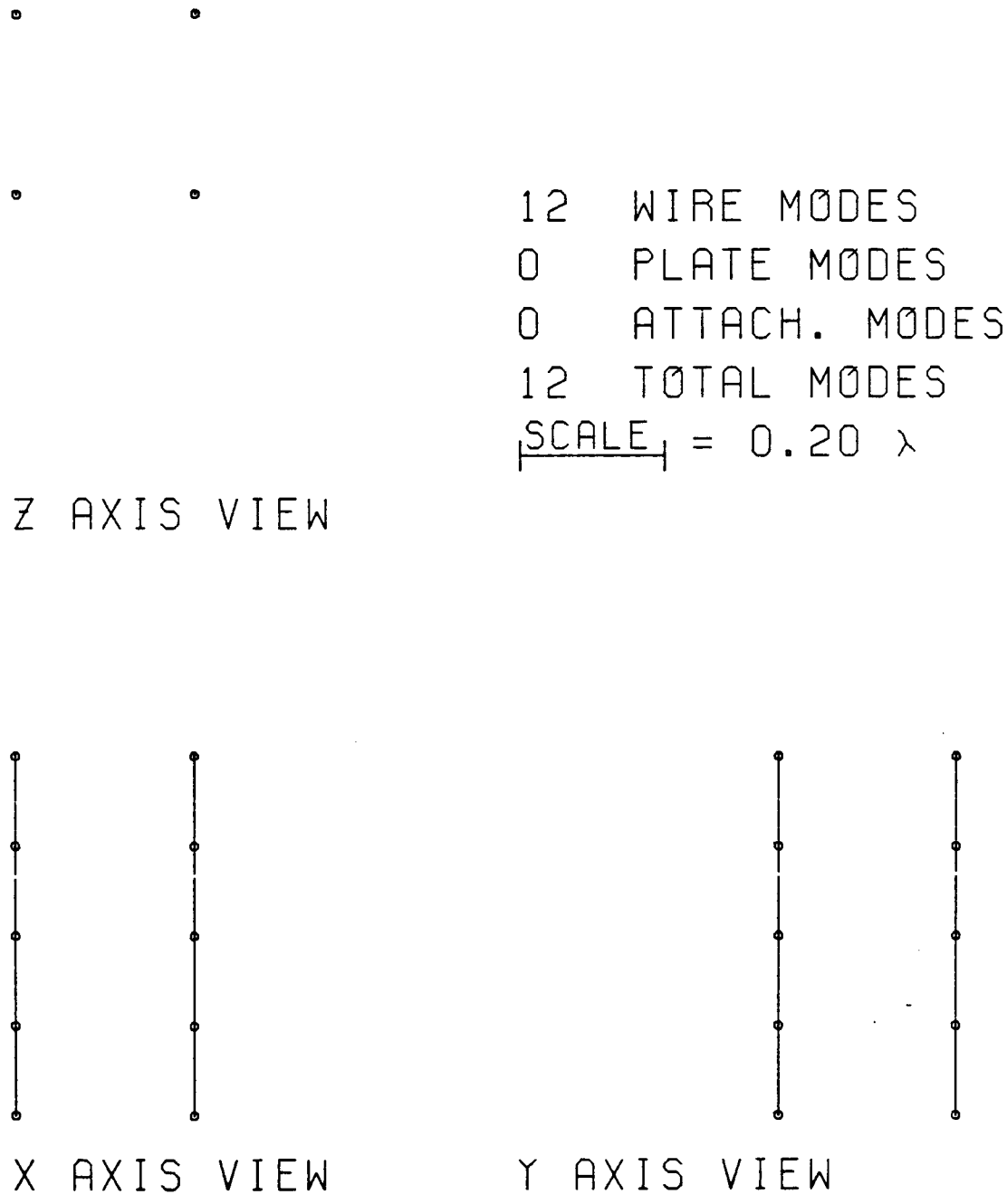

Figure 5.7. AOA antenna simulation geometry.

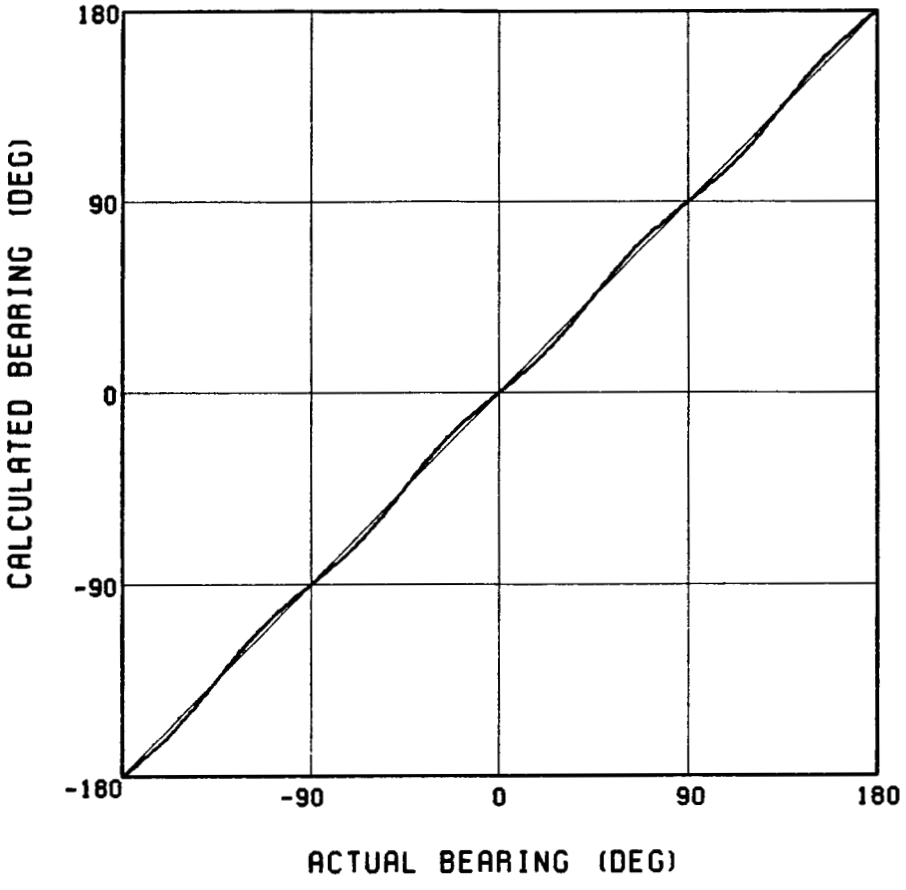

Figure 5.8. Calculated AOA transfer function using the ESP code.

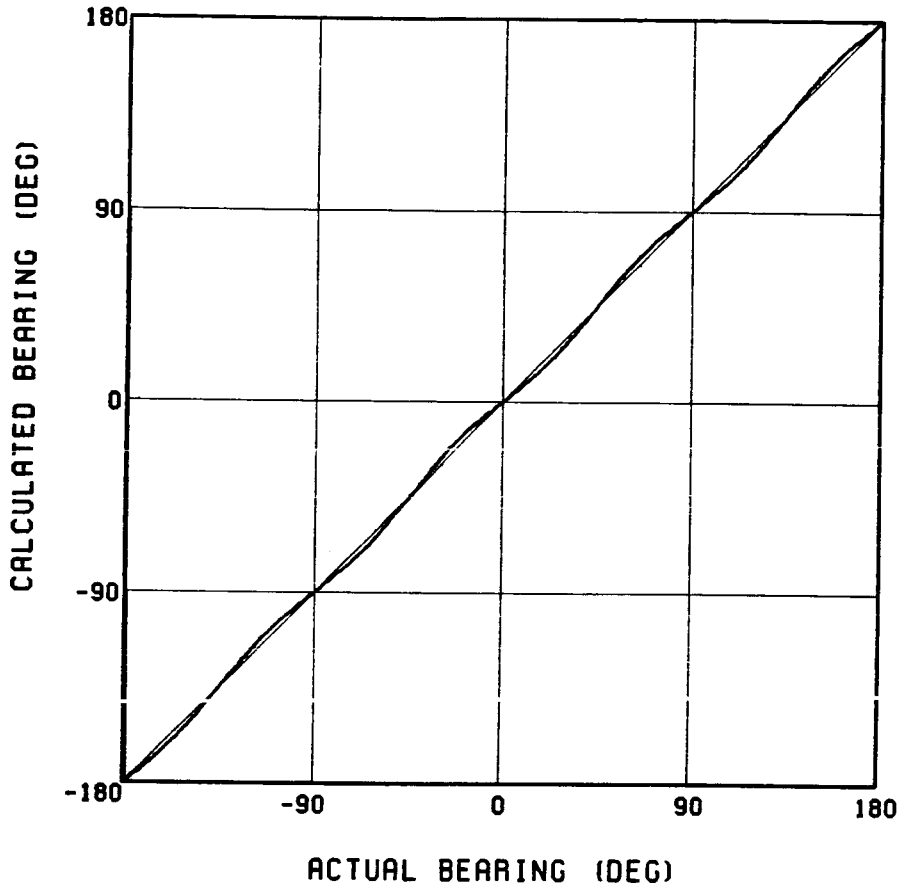

Figure 5.9. Calculated AOA transfer function using the BSC.

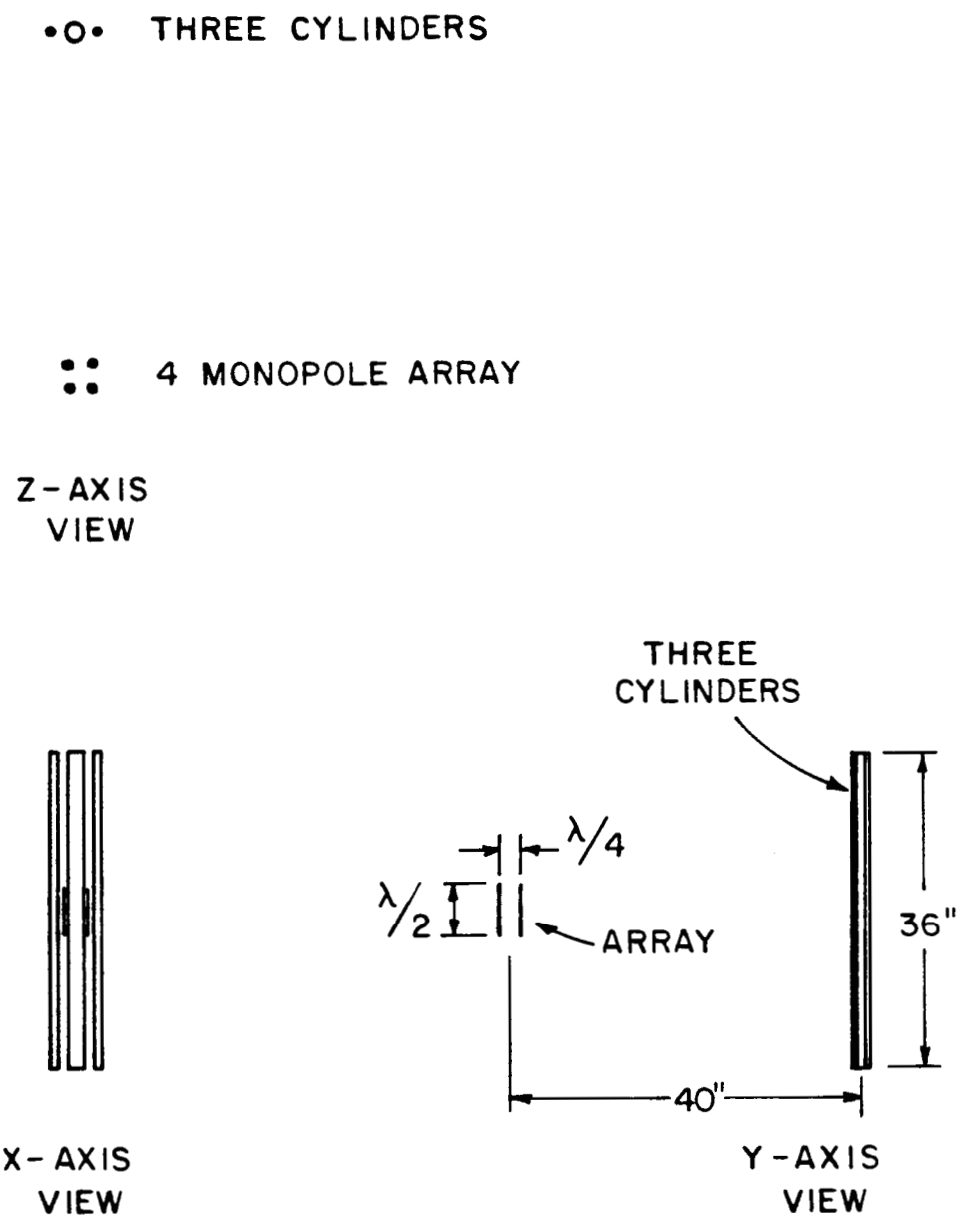

Figure 5.10. AOA antenna/cylinder geometry.

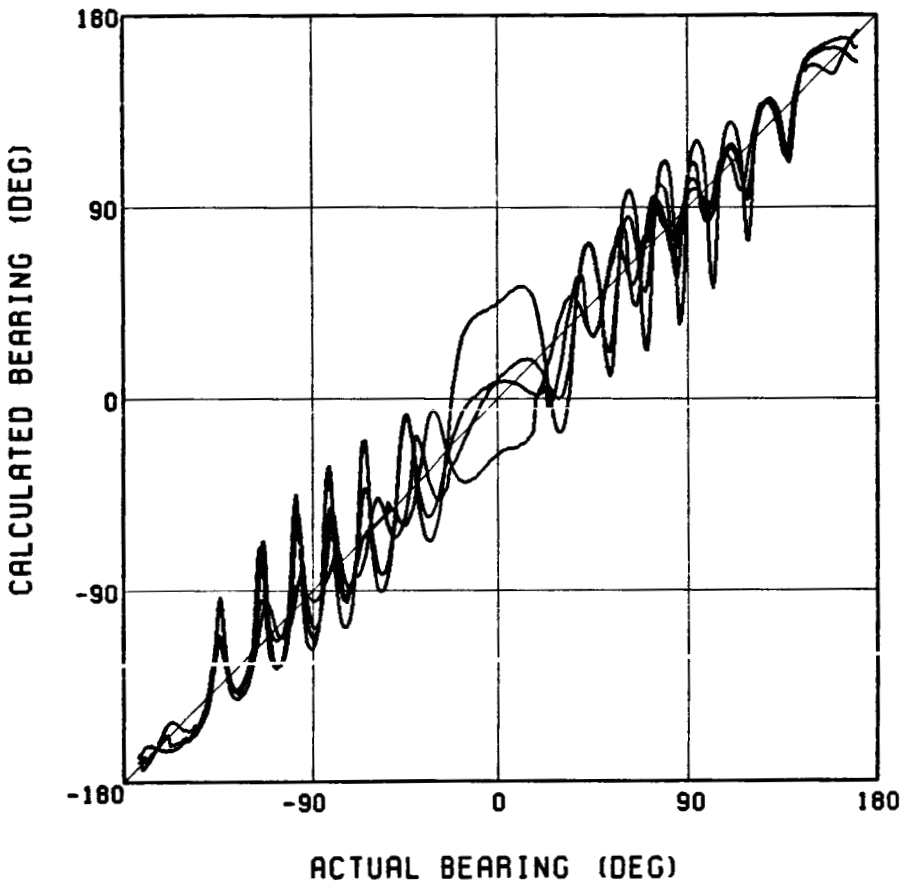

Figure 5.11. Calculated AOA performance in the presence of cylinders.

Since the spacing of the cylinders was small compared to the wavelength, the three cylinders were replaced with a plate and rotor blades were added to the computer model to determine their effects. The geometry is shown in Figure 5.12 using the BSC input file in Figure 5.13. The calculations were taken with the rotor shaft and blades rotated every 30 degrees. The results are overlayed in Figure 5.14.

Finally, the AOA performance was calculated at an elevation angle of 15 degrees above the horizon, so the signal would pass through the blades. The fields were calculated using the geometry shown in Figure 5.12 and with the rotor shaft and blades rotated every 30 degrees. The results are overlayed in Figure 5.15, and are similar to the previous ones.

The BSC provided a fairly accurate model of the AOA antenna system. It showed that without any scatterers, the system should be accurate within about 3 degrees (plus an offset). The model also showed that in the presence of scatterers, an undesireable amount of error is introduced. Finally, the model did well to simulated the results taken on the aircraft and in the anechoic chamber.

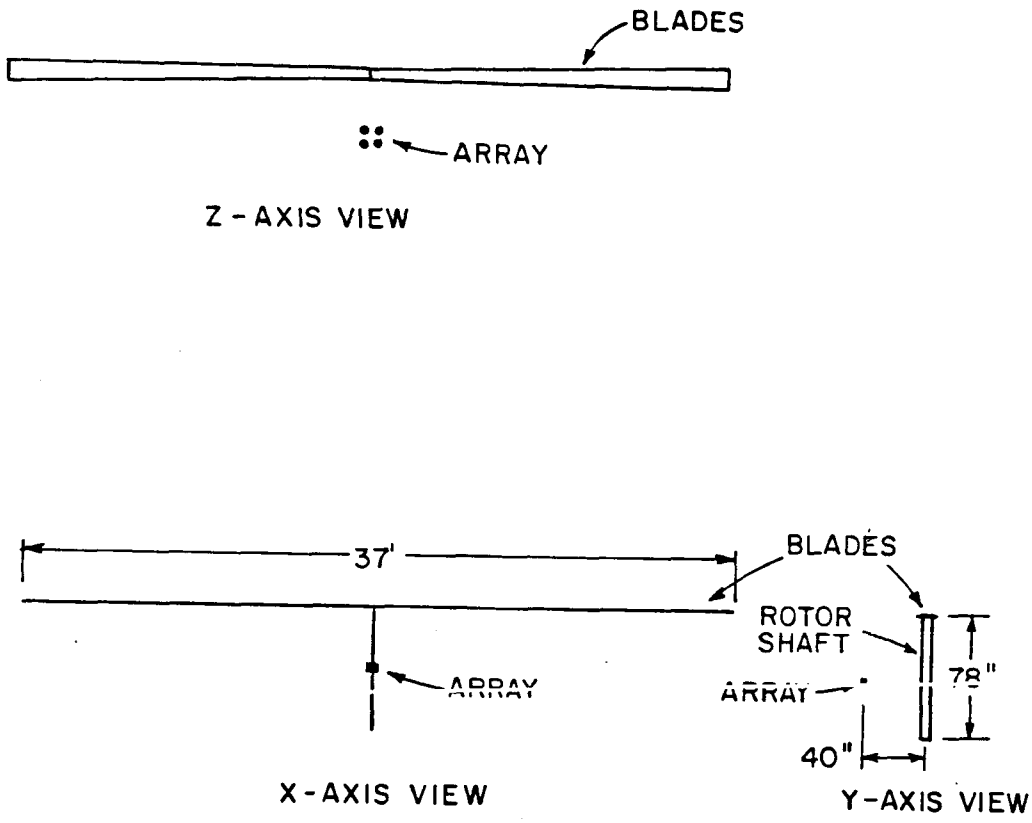

Figure 5.12. AOA antenna/rotor blade geometry.

```
CM:
CM: TCAS FOUR DIPOLE ARRAY
CE:
FR: FREQUENCY (GHZ)
1.090
PD: AZIMUTH PATTERN
0.,0.,90.,0.
T,90.0
0,360,1
US: SOURCE UNITS
0
UN: GEOMETRY UNITS
3
SG: DIPOLE A
1.35,1.35,0.0
0.,0.,90.,0.
-2,.5,0.
1.,0.
CM:
CM:  ROTATE ROTOR SHAFT & BLADES
CE:
RT:
-40.,0.,0.
0.,0.,90.,150.0
PG: PLATE
4,0
3.0,0.0,-39.
-3.0,0.0,-39.
-3.0,0.0,+39.
3.0,0.0,+39.
PG: BLADES
6,0
6.0,222.0,38.
4.0,0.0,38.
6.0,-222.0,38.
-6.,-222.,38.
-4.0,0.0,38.
-6.,222.,38.
LP:  LINE PRINTER
T
XQ:  EXECUTE
NS:
RT:  ORIGINAL ORIGIN
0.,0.,0.
0.,0.,90.,0.
SG:  DIPOLE B
-1.35,1.35,0.0
0.,0.,90.,0.
-2,.5,0.
1.,0.
XQ:  EXECUTE
NS:
SG:  DIPOLE C
-1.35,1.35,0.
0.,0.,90.,0.
-2,.5,0.
1.,0.
XQ:  EXECUTE
NS:
SG:  DIPOLE D
-1.35,1.35,0.
0.,0.,90.,0.
-2,.5,0.
1.,0.
XQ:  EXECUTE
EN:  END
```

Figure 5.13. AOA antenna/blade BSC input file.

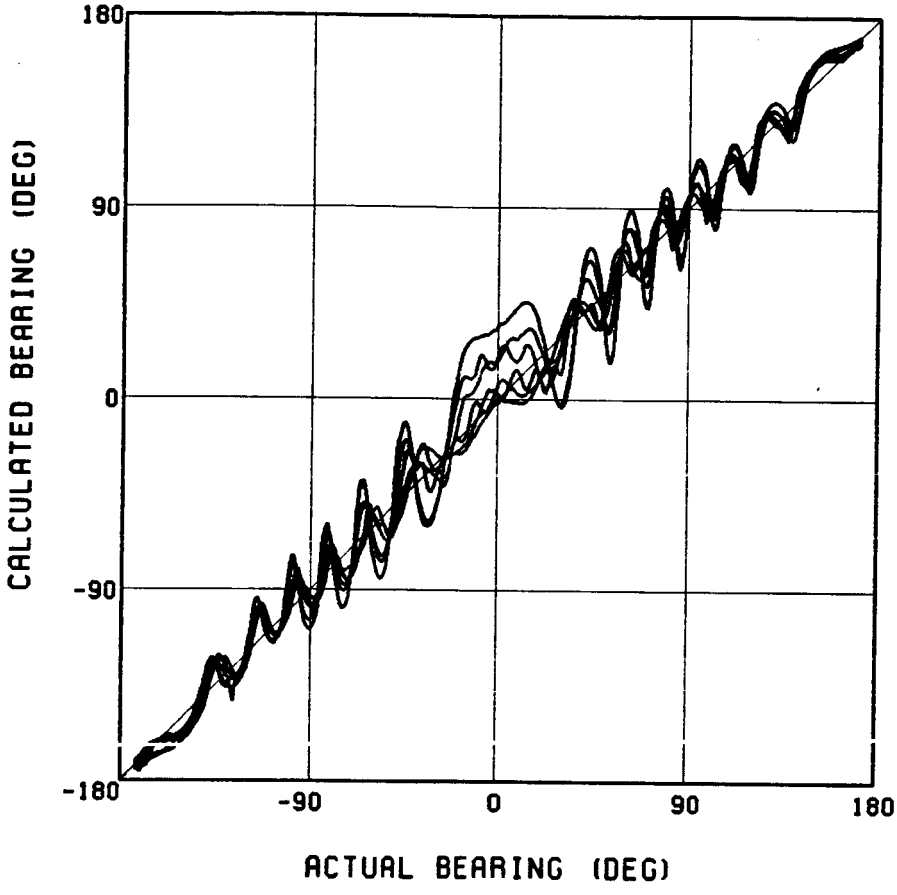

Figure 5.14. Calculated AOA antenna performance in the presence of shaft and blades.

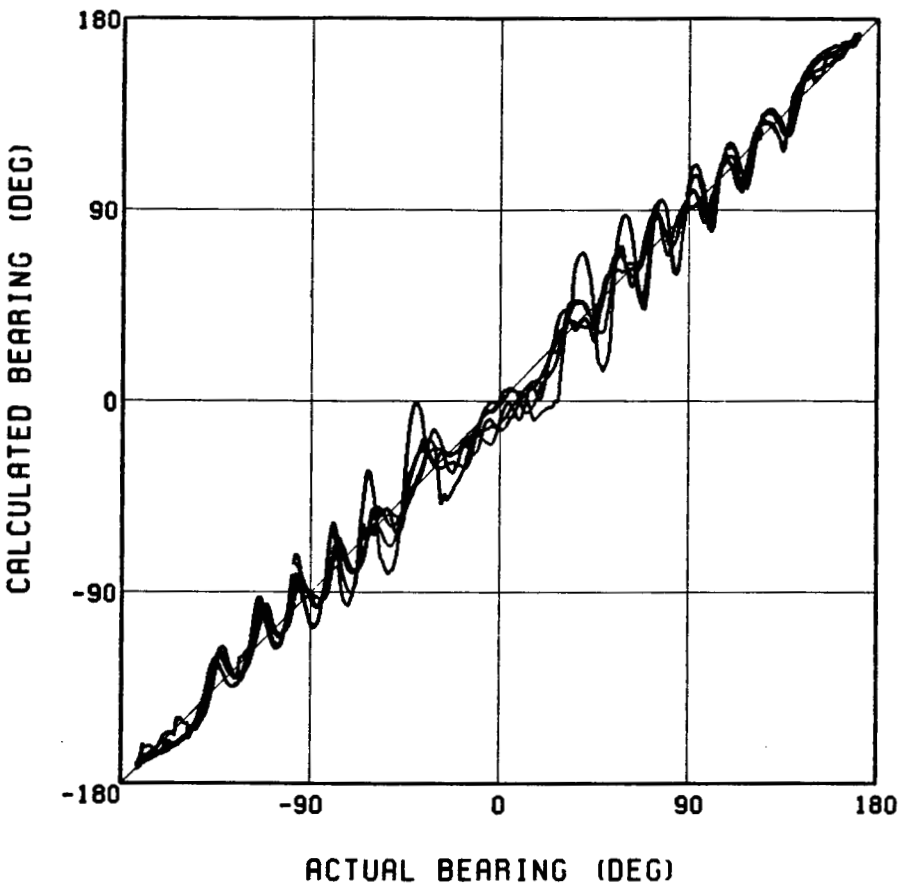

Figure 5.15. Calculated AOA antenna performance 15 degrees above the aircraft horizon.

CHAPTER VI

SUMMARY AND CONCLUSIONS

The purpose of this study was to develop accurate computer models of various aircraft and antenna systems. Three computer codes were utilized; the Airborne Antenna Code, the Basic Scattering Code, and the Electromagnetic Surface Patch Code.

An L-band antenna installed on a P-3B aircraft was analyzed using the Airborne Antenna Code. The aircraft fuselage was modelled as an ellipsoid with plates added to model the wings, horizontal stabilizers and engine housings. The ESP code was also used in the model to determine the current induced on a marker beacon located behind the antenna. This current was input into the Airborne Antenna Code as a second source. Results showed very good agreement with measured results.

A UHF relay pod on an A-7E aircraft was also analyzed using the Airborne Antenna Code. This time the pod was modelled as an ellipsoid and the wing, pod mount, horizontal stabilizer and the side of the aircraft were modelled by plates. The ESP code was again used because three other antennas were located on the pod. The currents induced on the three antennas were calculated using the ESP code and input into the

Airborne Atnenna Code. The diameter of the ellipsoid was less than a wavelength which may be pushing the accuracy of the code, but the calcualted results did well to show the lobing and blockage caused by the side of the aircraft.

Finally, a traffic advisory system installed on a Bell Long Ranger helicopter was analyzed using the Basic Scattering Code. Cylinders were used to model the rotor shaft which was located behind a four-element array of momopole antennas. Later, the cylinders were replaced by a plate and additional plates were added to simulate the rotor blades. The array was connected to a hybrid network which determined the angle-of-arrival of an incoming signal. The BSC was used to calculate the angle-of-arrival, and the results were compared to measured results. The BSC provided a fairly accurate model of the AOA antenna system and did well to shown the error introduced by the rotor shaft and blades.

The Airborne Antenna Code, Basic Scattering Code and Electromagnetic Surface Patch Code provide powerful tools for predicting the performance of airborne antenna systems. These codes can be very useful in the design stage of an antennas system to determine the optimum antenna location. Valuable time and costly flight-hours could be saved by first using these codes.

REFERENCES

[1] R.G. Kouyoumjian and P.H. Pathak, "A Uniform Geometrical Theory of Diffraction for an Edge in a Perfectly-Conducting Surface," Proc. IEEE, Vol. 62, pp. 1448-1461, November 1974.

[2] R.G. Kouyoumjian, P.H. Pathak and W.D. Burnside, "A Uniform GTD for the Diffraction by Edges, Vertices and Convex Surfaces," Theoretical Methods for Determining the Interaction of Electromagnetic Waves with Structures, Edited by J.K. Skwirynski, Sijthoff, and Nordhoff, Netherlands, 1978.

[3] P.H. Pathak, N. Wang, W.D. Burnside and R.G. Kouyoumjian, "A Uniform GTD Solution for the Radiation from Sources on a Convex Surface," IEEE Trans. on Antenna and Propagation, Vol. AP-29, No. 4, pp. 609-622, July 1981.

[4] Hsin-Hsien Chung and W.D. Burnside, "General 3D Airborne Antenna Radiation Pattern Code User's Manual," Technical Report 711679-10, The Ohio State University ElectroScience Laboratory, Department of Electrical Engineering, prepared under Contract No. F30602-79-C-0068 for Rome Air Development Center, July 1982.

[5] R.J. Marhefka and W.D. Burnside, "Numerical Electromagnetic Code-Basic Scattering Code (Version 2), Part I: User's Manual", Technical Report 712242-14, The Ohio State University, ElectroScience Laboratory, Department of Electrical Engineering, prepared under Contract NO0123-79-C-1469 for Naval Regional Contracting Office, December 1982.

[6] R.J. Marhefka, "Numerical Electromagnetic Code-Basic Scattering Code (Version 2), Part II: Code Manual," Technical Report 712242-15, The Ohio State university, ElectroScience Laboratory, Department of Electrical Engineering, prepared under contract NO0123-79-C-1469 for Naval Regional Contracting Office, December 1982.

[7] E.H. Newman, "A User's Manual for: Electromagnetic Surface Patch Code (ESP)" Technical Report 713402-1, The Ohio State University, ElectroScience Laboratory, Department of Electrical Engineering, prepared under Grant No. DAAG-29-81-K-0020 for U.S. Army Research Office, July 1981.